CANCER

Target antigen–displaying extracellular vesicles boost CAR T cell efficacy in cell and mouse models of neuroblastoma

Anna Maria Giudice[1], Stephanie Matlaga[1], Sydney L. Roth[1], Guillem Pascual-Pasto[1], Patrick M. Schürch[1], Geoffrey Rouin[1], Brendan McIntyre[1], Grant P. Grothusen[1], Evan Cresswell-Clay[1,2], Rawan Shraim[1,2], David Groff[1], Vincent Zecchino[1], Simona Lombardi[1], Daniel Martinez[3], Lynn A. Spruce[4], Elizabeth M. Brown[4], Hossein Fazelinia[2,4], Sarah E. Henrickson[5,6], Jonas Nance[7], C. Patrick Reynolds[7], Kristopher R. Bosse[1,6]*

Glypican-2 (GPC2) and the disialoganglioside GD2 are validated CAR T cell targets in neuroblastoma, but durable clinical responses remain limited. This modest chimeric antigen receptor T cell (CAR T cell) efficacy is in part due to suboptimal T cell persistence, antigen down-regulation, and a hostile tumor microenvironment, which includes immune cell–modulating extracellular vesicles (EVs). Neuroblastoma-derived EVs may contain CAR targets or other immunoregulatory elements that can modulate CAR T cell antitumor activity. Thus, we first profiled the surfaceome of neuroblastoma EVs and assessed their impact on both GPC2 and GD2 CAR T cell function. Neuroblastoma EVs displayed GPC2 and GD2, with minimal expression of programmed death-ligand 1 (PD-L1), and were detected in blood from tumor-bearing mice and patients. These EVs directly activated paired CAR T cells, suggesting a role for a peripheral source of CAR antigen. To exploit this therapeutically, we engineered nontumor-derived GPC2+ synthetic EVs (SyntEVs) as CAR T cell enhancers and armored them with either albumin-binding domains or GD2-binding domains. In mice harboring human neuroblastoma cell line–derived or patient-derived xenografts, serial infusion of armored SyntEVs after GPC2 CAR T cells enhanced tumor control by boosting peripheral CAR T cell persistence. Moreover, GD2-targeting SyntEVs decorated low-antigen tumor cells with GPC2, circumventing antigen down-regulation. This SyntEV platform offers a versatile system to address the therapeutic limitations of CAR T cells in solid tumors.

INTRODUCTION

Chimeric antigen receptor T cell (CAR T cell) therapy has demonstrated remarkable success in treating patients with hematological malignancies (*1*). Despite these advances, early clinical studies in patients with solid tumors have generally fallen short of achieving similar sustained clinical responses, even when the targeted antigens are differentially and abundantly expressed (*2*). Barriers to the effectiveness of CAR T cells in solid tumors include antigen heterogeneity (*3*), limited CAR T cell persistence, and immunoregulation induced by the tumor microenvironment (TME) (*2*, *4*), in which intercellular messengers such as tumor-derived extracellular vesicles (TEVs) contribute to the complex cross-talk between tumor and immune cells. TEVs are nanosized lipid-bilayer vesicles secreted by cancer cells that carry bioactive molecules, including immunoregulatory proteins such as immune checkpoint ligands (*5*, *6*), major histocompatibility complex (MHC) molecules, and tumor-associated antigens (*7*), with the ability to diversely modulate interacting cells depending on their cargo composition (*8*). For example, EVs may exhibit immunogenic properties such as transferring antigen to dendritic cells (DCs) inducing cytotoxic T lymphocyte activation (*9*). Conversely, EVs carrying inhibitory checkpoint molecules, such as Fas ligand (*10*) and programmed death-ligand 1 (PD-L1) (*6*), or immunosuppressive cytokines can potently inhibit immune cells (*11*). Moreover, the EV surfaceome can influence the clinical response to immunotherapeutics, including monoclonal antibodies (*12*), antibody-drug conjugates (*13*), and CAR T cells (*14*). For example, EVs that harbor therapeutic antibody target molecules can act as a decoy facilitating tumor cell evasion, such as what has been observed with PD-L1–positive (PD-L1+) EVs sequestering anti–PD-L1 antibodies in melanoma and lung cancer (*5*, *6*). In the context of CAR T cell therapy, studies in hematological malignancies suggest that CD19 CAR T cell dysfunction can be induced by tumor-derived EVs because of the concomitant presence of the target antigen CD19 and PD-L1 (*7*). However, how immunotherapeutic target antigens on EVs modulate CAR T cell functionality in solid tumors, especially those with limited PD-L1 expression like neuroblastoma (*15*), is not well known. Furthermore, whether manipulation of EV cargo can confer therapeutically beneficial immunostimulatory properties and serve as CAR T cell adjuvants also remains unexplored.

High-risk neuroblastoma is an unrelenting childhood cancer with long-term survival below 50% despite intensive multimodal chemoradiotherapy (*16*), with a critical need for innovative treatments. Our lab has identified glypican-2 (GPC2) as a differentially expressed immunotherapeutic target in high-risk neuroblastoma and other lethal cancers with no substantial expression on vital normal tissues (*17*).

[1]Division of Oncology and Center for Childhood Cancer Research, Children's Hospital of Philadelphia, Philadelphia, PA 19104, USA. [2]Department of Biomedical and Health Informatics, Children's Hospital of Philadelphia, Philadelphia, PA 19104, USA. [3]Department of Pathology, Children's Hospital of Philadelphia, Philadelphia, PA 19104, USA. [4]Proteomics Core Facility, Children's Hospital of Philadelphia, Philadelphia, PA 19104, USA. [5]Division of Allergy and Immunology, Children's Hospital of Philadelphia, Philadelphia, PA 19104, USA. [6]Department of Pediatrics, Perelman School of Medicine at the University of Pennsylvania, Philadelphia, PA 19104, USA. [7]Pediatric Cancer Research Center and Department of Pediatrics, School of Medicine, Texas Tech University Health Sciences Center, Lubbock, TX 79430, USA.
*Corresponding author. Email: bossek@chop.edu

We and others have isolated high-affinity GPC2 binders and developed effective immunotherapies targeting this molecule, including potent and safe second-generation GPC2 CAR T cells (*18*–*22*), one of which is currently being tested in a first-in-human phase 1 clinical trial (NCT05650749). Several clinical trials are also evaluating the safety and efficacy of GD2 CAR T cells in children with neuroblastoma and other GD2-positive tumors (*23*–*25*), work that recently provided the first convincing evidence that CAR T cells can be effective for this pediatric embryonal tumor (*23*). However, similar to other potent CARs and solid tumor histologies, down-regulation of the targeted antigen under CAR pressure (*3*, *21*), limited CAR T cell persistence, and a hostile immunosuppressive TME (*26*, *27*) drive CAR T cell resistance. Collectively, these data suggest that CAR vaccination strategies that deliver more accessible CAR ligand, for example, by providing antigen+ EVs outside of the immunosuppressive TME, may be an effective strategy to reinvigorate CAR T cells in the setting of limited T cell persistence or antigen down-regulation to ultimately achieve more durable clinical responses.

In this study, we deepen our understanding of the neuroblastoma EV surfaceome and the interaction between TEVs and CAR T cell therapies in this disease, along with providing proof of concept for using antigen-displaying synthetic EVs (SyntEVs) as a therapeutic platform to enhance clinically available solid tumor CAR T cell therapies.

RESULTS

GPC2 and other immunotherapeutic targets are selectively exposed on neuroblastoma-derived EVs

First, to define the protein cargo of neuroblastoma EVs, we isolated EVs from seven human neuroblastoma and two nontumor control cell lines using ultracentrifugation (*28*). Transmission electron microscopy (TEM) of isolated EVs confirmed the presence of vesicle-shaped particles in the range of 50 to 300 nm in diameter (Fig. 1A), which was verified by Nanoparticle Tracking Analysis (NTA; Fig. 1B). EV secretion kinetics were evaluated across all cell lines, showing that EV abundance was significantly higher in neuroblastoma cells compared with nontumor control cells ($P < 0.05$; fig. S1A). Neuroblastoma EV–associated proteins were then characterized by immunoblotting, confirming the presence of small EV (sEV) markers CD81 and Alix and the absence of calnexin in all EV isolations [fig. S1B; (*29*)]. Neuroblastoma-associated antigens, including neural cell adhesion molecule 1 (NCAM1), L1 cell adhesion molecule (L1CAM), GPC2, and B7 homolog 3 (B7-H3), were exclusively present in EVs isolated from neuroblastoma cell lines but not in EVs released by a nontumor control cell line (Fig. 1C). Furthermore, neuroblastoma-specific cell surface molecules such as GD2, GPC2, and NCAM1 were identified by flow cytometry exclusively on the surface of neuroblastoma EVs (Fig. 1, D and E), whereas CD81 abundance was comparable across all EV isolates. Neuroblastoma-derived EVs contained minimal amounts of PD-L1, with only EVs from the SK-N-AS cell line having any appreciable PD-L1 exposure (Fig. 1C and fig. S1C). However, SK-N-AS EV PD-L1 abundance was modest compared with those reported on TEVs from other cancers (*5*, *30*) even after 48 hours of coincubation with interferon-γ (IFN-γ), conditions that are known to markedly up-regulate both parent cell and EV PD-L1 (*5*), as we observed in control melanoma WM164 cells (Fig. 1C and fig. S1C). Last, to more globally define the neuroblastoma EV protein cargo composition, we performed mass spectrometry (MS) on EVs isolated from two distinct neuroblastoma cell lines, the adrenergic NB-EbC1 cell line and more mesenchymal SK-N-AS cells (*31*). Neuroblastoma cell heterogeneity and plasticity are best exemplified by the recent characterization of both adrenergic and mesenchymal cell states in neuroblastoma preclinical models and tumors (*32*, *33*), which are epigenetically distinct but interchangeable and can exhibit substantially different surfaceomes (*34*–*36*). MS identified a total of 4543 proteins, with 56.8% shared between NB-EbC1 and SK-N-AS EVs (Fig. 1F). High abundance of neuroblastoma cell surface molecules was detected in neuroblastoma-derived EVs, including proteins present in EVs from both cell lines, such as B7-H3, GPC2, cell adhesion molecule 1 (CADM1), vimentin (VIM), and GDNF family receptor alpha 2 (GFRA2) (Fig. 1G, top). These MS studies also confirmed low abundance of inhibitory checkpoint ligands on neuroblastoma EVs, such as PD-L1 (CD274) and poliovirus receptor (PVR; Fig. 1G, middle), with many others being undetectable, and the expected presence of sEV markers (CD63, CD81, and CD9; Fig. 1G, bottom). Last, other proteins displayed differential EV abundance, largely reflecting the cell state–specific surfaceome (*31*, *36*, *37*). Specifically, proteins associated with an adrenergic phenotype, such as solute carrier family 6 member 2 (SLC6A2), Delta-like noncanonical Notch ligand 1 (DLK1), anaplastic lymphoma kinase (ALK), and L1CAM, were enriched in NB-EbC1 TEVs (Fig. 1H, top). Proteins linked to a more mesenchymal phenotype, such as CD44, platelet-derived growth factor receptor alpha (PDGFRA), EPH receptor A2 (EPHA2), Erb-b2 receptor tyrosine kinase 2 (ERBB2), and AXL receptor tyrosine kinase (AXL), were alternatively found in higher abundance in SK-N-AS TEVs (Fig. 1H, bottom). Together, neuroblastoma EVs are enriched in immunotherapeutic target molecules such as GPC2 and GD2 but display low PD-L1 and other inhibitory checkpoint ligands, which contrasts with TEVs from other tumor histologies where PD-L1 abundance is more predominant (*5*, *14*).

Circulating GPC2+ and GD2+ EVs are present in neuroblastoma-bearing mice and patients

Tumor-derived EVs can be detected in the peripheral blood of patients with cancer as circulating EVs (circEVs), several of which directly modulate immunotherapeutic efficacy (*12*, *30*) or have demonstrated diagnostic utility (*38*, *39*). Considering the recent focus of targeting GPC2 and GD2 with CAR T cells and other immunotherapies (*18*–*23*), we first investigated whether neuroblastoma-derived GPC2+ or GD2+ circEVs can be detected in the peripheral blood of neuroblastoma-bearing mice or humans. We established six human neuroblastoma patient-derived xenografts (PDXs) in severe combined immunodeficient (SCID) mice. When PDX tumors reached a volume of 2 cm^3, EVs were isolated from the peripheral blood and assessed for EV particle count by NTA and for GPC2 and GD2 abundance with flow cytometry (fig. S1D). Peripheral blood from mice with human neuroblastoma PDXs contained a higher number of circEVs compared with nontumor-bearing mice but with no difference in particle size between the groups (fig. S1, E and F). Moreover, GPC2 and GD2 were selectively detected on circEVs from mice harboring neuroblastoma PDXs (Fig. 2, A and B), and the abundance of GPC2+ EVs isolated from each mouse correlated with the expression of GPC2 in the parent tumor ($R^2 = 0.3$, $P = 0.005$ Fig. 2A and fig. S1, G and H). Although GD2+ EVs were also selectively isolated from tumor-bearing mice, the amount of GD2+ EVs did not correlate as well with parent tumor GD2 [coefficient of determination (R^2) = 0.13, $P = 0.072$; Fig. 2B and fig. S1, G and H]. No

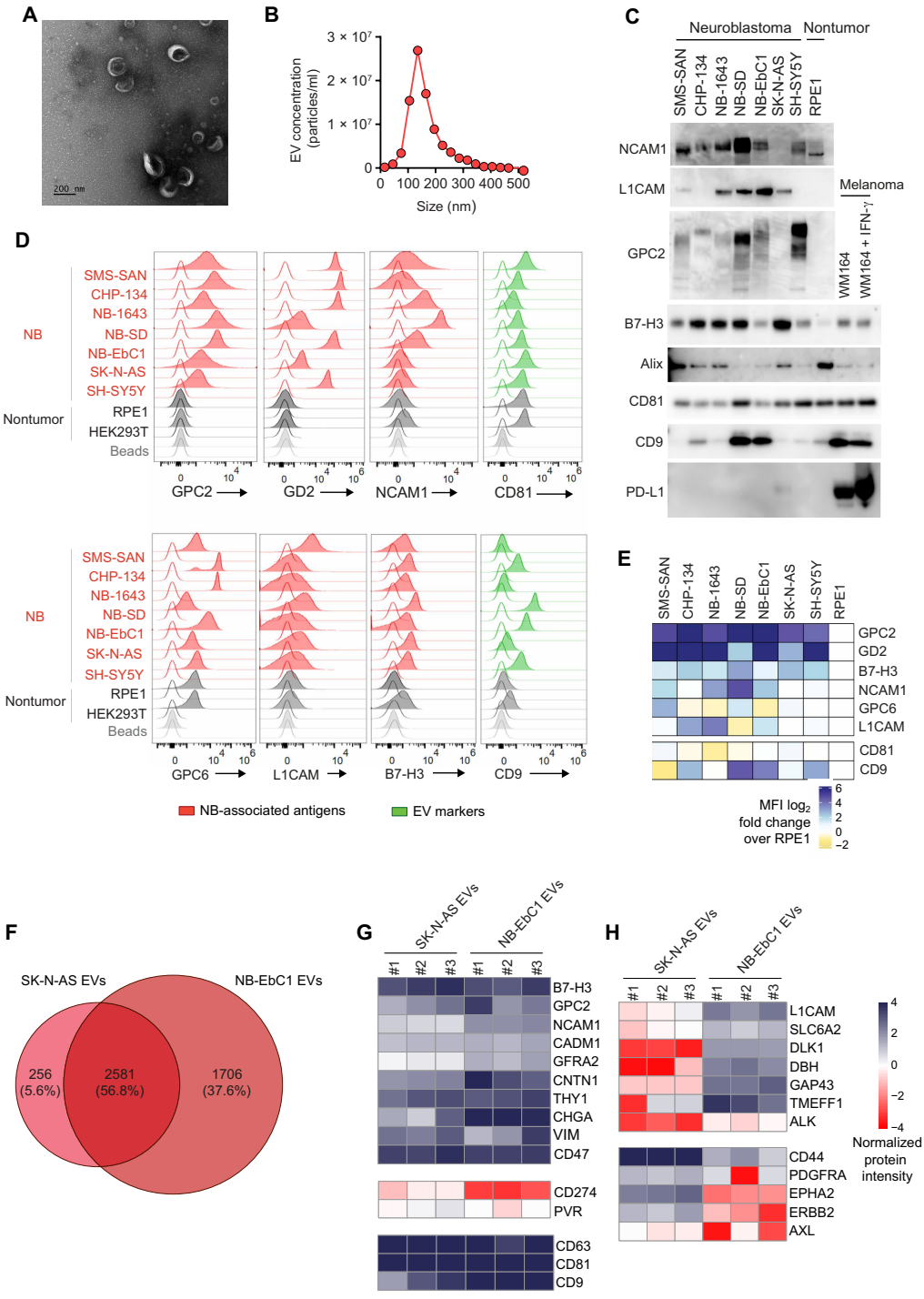

Fig. 1. Neuroblastoma cells release EVs carrying GPC2, GD2, and other tumor-associated antigens. (**A** and **B**) Representative characterization of EVs isolated from SK-N-AS cells by TEM (A) and NTA (B). Scale bar in (A), 200 nm. (**C**) Western blot of EVs isolated from neuroblastoma, nontumor RPE1, and melanoma WM164 cell lines. Neuroblastoma-associated antigens (NCAM1, L1CAM, GPC2, and B7-H3), sEV markers (Alix, CD81, and CD9), and PD-L1 are shown. Equal amounts of total protein were loaded for each sample. (**D**) Surface expression of neuroblastoma-associated and sEV-associated molecules on bead-bound EVs isolated from seven neuroblastoma (NB) and two nontumor cell lines by flow cytometry. Filled colored plots represent staining with the antibody indicated on the *x* axis, and empty plots represent unstained samples. (**E**) Heatmap showing the surface exposure of tumor antigens on neuroblastoma-derived EVs as fold change over nontumor RPE1 EVs. MFI, mean fluorescence intensity. (**F**) Venn diagram showing proteins identified in SK-N-AS and NB-EbC1 EVs by MS ($n = 3$ biological replicates). Common and exclusive proteins identified from the SK-N-AS and NB-EbC1 EVs are shown as overlapping and nonoverlapping areas, respectively, with the numbers of total proteins (and percentages) indicated. (**G**) Heatmap showing the MS normalized protein intensity for proteins of interest from SK-N-AS and Nb-EbC1 EVs ($n = 3$ biological replicates). Neuroblastoma cell surface molecules (top), inhibitory checkpoint ligands (middle), and sEV markers (bottom) are shown. (**H**) Heatmap showing the MS normalized protein intensity for adrenergic (top) and mesenchymal (bottom) proteins of interest from SK-N-AS and Nb-EbC1 EVs.

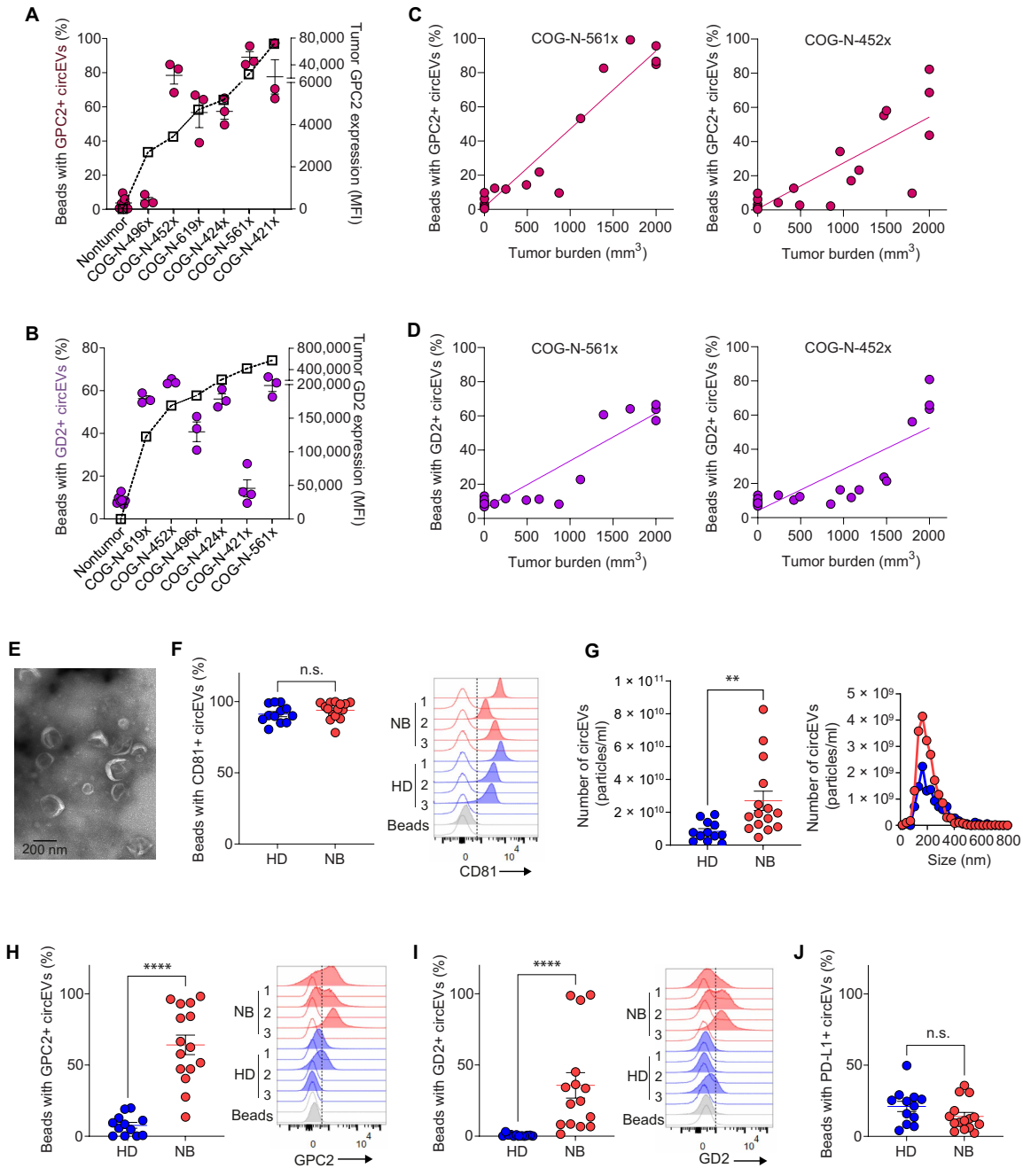

Fig. 2. Circulating GPC2+/GD2+ EVs are detectable in the peripheral blood of tumor-bearing mice and patients with neuroblastoma. (**A**) Association between the percentages of circulating GPC2+ bead-conjugated EVs (magenta-colored dots; left *y* axis) and tumor GPC2 expression (black squares; right *y* axis) from neuroblastoma PDX–bearing mice. (**B**) Association between the percentages of circulating GD2+ bead-conjugated EVs (purple-colored dots; left *y* axis) and tumor GD2 expression (black squares; right *y* axis) from neuroblastoma PDX–bearing mice. (**C** and **D**) Correlation between the percentages of circulating GPC2+ (C) and GD2+ (D) bead-conjugated EVs and tumor size (COG-N-561x, $n = 12$; COG-N-452x, $n = 13$). (**E**) Representative TEM image of circEVs derived from a patient with neuroblastoma. Scale bar, 200 nm. (**F**) Left: Comparison of the percentages of CD81+ bead-conjugated EVs between patients with neuroblastoma (red, $n = 15$) and healthy children (blue, $n = 12$). Right: Representative CD81 flow cytometry histograms. (**G**) Left: Comparison of the amounts of circEVs between patients with neuroblastoma (red, $n = 15$) and healthy children (blue, $n = 12$). Right: Representative particle size distribution by NTA between circEVs from a patient with neuroblastoma (red) and a healthy child (blue). (**H**) Left: Comparison of the percentages of GPC2+ bead-conjugated EVs between patients with neuroblastoma (red, $n = 15$) and healthy children (blue, $n = 12$). Right: Representative GPC2 flow cytometry histograms. (**I**) Left: Comparison of the percentages of GD2+ bead-conjugated EVs between patients with neuroblastoma (red, $n = 15$) and healthy children (blue, $n = 12$). Right: Representative GD2 flow cytometry histograms. (**J**) Comparison of the percentages of PD-L1+ bead-conjugated EVs between patients with neuroblastoma (red, $n = 15$) and healthy children (blue, $n = 12$). For each flow cytometry plot, filled colored plots represent staining with the antibody indicated on the *x* axis and empty plots represent unstained samples. Data are shown as means ± SEM. Dots represent individual mice [(A) to (D)] or human patients [(F) to (J)]. Statistical analysis was performed using simple linear regression to assess correlation between GPC2/GD2 expression on circEVs and tumor samples [(A) to (D)] or Mann-Whitney test to evaluate difference between two groups [(F) to (J)]. $^{**}P < 0.01$; $^{****}P < 0.0001$; n.s., not significant.

PD-L1 was detected on PDX-circEVs (fig. S1I). Last, isolation of EVs from the peripheral blood of PDX-bearing mice with various tumor sizes revealed that the abundance of both GPC2+ and GD2+ circEVs significantly correlated with the overall tumor burden (Fig. 2, C and D; GPC2, $R^2 = 0.92$ for COG-N-561x; $R^2 = 0.82$ for COG-N-452x; GD2, $R^2 = 0.86$ for COG-N-561x, and $R^2 = 0.70$ for COG-N-452x; all $P < 0.0001$).

To validate these data, we next determined whether GPC2+ or GD2+ EVs could be selectively isolated from the peripheral blood of children with neuroblastoma. We isolated EVs from archived peripheral blood samples from 15 patients with neuroblastoma and 12 age-matched healthy controls. TEM analysis of purified human circEVs revealed the presence of vesicle-shaped particles consistent with EVs (Fig. 2E), and flow cytometry showed comparable CD81 positivity between the two cohorts (Fig. 2F). However, the relative concentration of circEVs by NTA was significantly higher in the peripheral blood of children with neuroblastoma compared with healthy donors (Fig. 2G), similar to what we observed in our PDX models and validating what has been observed in other oncology patient cohorts (*38*, *40*). No difference in particle size between the two cohorts was observed (fig. S1J). However, EVs isolated from the peripheral blood of children with neuroblastoma again selectively showed high abundance of GPC2 and GD2 ($P < 0.0001$; Fig. 2, H and I), whereas they did not have substantial PD-L1 (Fig. 2J and fig. S1K). Together, these studies show that GPC2 and GD2 are selectively found on circEVs from mice and children with neuroblastoma. In mice with neuroblastoma, the abundance of GPC2+ and GD2+ circEVs correlates with both disease burden and at least partially with parent tumor cell GPC2/GD2 expression. These studies also suggest a potential role for GPC2+ and GD2+ circEVs as noninvasive diagnostic biomarkers in children with neuroblastoma.

Target antigen+ EVs bind and activate CAR T cells in an antigen-dependent manner

Our findings of clinically relevant tumor-associated immunotherapeutic targets (*23*) on neuroblastoma-derived EVs motivated us to investigate how these target+ EVs might modulate the functionality of paired CAR T cells. We first focused on GPC2 given the recent development of several safe and effective CAR T cells (*18*, *20*, *21*), one of which is being tested in an early phase trial (NCT05650749). To enable these studies, we first generated SK-N-AS–GPC2 and human embryonic kidney (HEK) 293T–GPC2 isogenic cell lines (fig. S2A) as a source of GPC2+ EVs with different densities of target antigen (ultrahigh/high/low/negative). The expected variable EV surface GPC2 was validated by flow cytometry, which also revealed lack of the inhibitory checkpoint molecule PD-L1, whose presence on the EV surface has been previously linked with CAR T cell inhibitory effects (*14*) (Fig. 3A). Using human primary T cells, we generated GPC2-targeting CAR T cells with either CD28 or 4-1BB costimulatory domains (GPC2.28z and GPC2.BBz, respectively) and CD19 CAR T cells as a nontargeting control as described previously (fig. S2, B and C) (*20*).

First, we studied the interaction of $GPC2^{UltraHigh/High/Low/Neg}$ EVs with GPC2.28z CAR T cells by performing coincubation studies using EVs fluorescently labeled with PKH67, followed by flow cytometry binding assays and fluorescence microscopy (Fig. 3, B and C). For each EV sample, NTA was first performed, and the same number of particles was used in T cell coincubation assays across the different EV samples. Here, we observed that GPC2+ EVs selectively bind to the CAR+ subset of T cells and that the percentage of EV-bound CAR T cells varied in an EV antigen density–dependent manner, whereas no differences in EV binding were observed for the CAR− T cell subset or control CD19 (nontargeting) CAR T cells (fig. S2, D and E). We additionally noted a concentration-dependent effect of EVs on the interaction with GPC2 CAR T cells across all EV subsets (Fig. 3D).

We next evaluated the functional effects of GPC2+ EV binding to GPC2 CAR T cells in 24-hour coincubation assays. In these studies, GPC2+ EVs activated GPC2.28z CAR T cells in an antigen-dependent manner, as shown by increased expression of CD69 and granzyme B on the CAR+ T cell subset (Fig. 3E) along with increased interleukin-2 (IL-2) and IFN-γ secretion by GPC2+ EV–stimulated CAR T cells (Fig. 3, F and G). Comparable magnitudes of GPC2+ EV–induced GPC2 CAR T cell activation were observed with GPC2.BBz CAR T cells, suggesting that the GPC2+ EV/CAR T cell intersection is independent of the CAR costimulatory domain (fig. S2, F and G).

Next, the target cell cytotoxicity of EV-primed GPC2 CAR T cells was tested using three luciferase-tagged neuroblastoma cell lines with different amounts of cell surface GPC2. When coincubated for 24 hours, GPC2+ EV–primed GPC2 CAR T cells were substantially more cytotoxic to target neuroblastoma cells compared with unstimulated CAR T cells or CAR T cells preincubated with $GPC2^{Neg}$ EVs (Fig. 3H and fig. S2H). This enhanced CAR T cell cytotoxicity was again independent of CAR costimulatory domain (fig. S2I). Last, as further proof that EV-induced GPC2 CAR T cell activation is not due to nonspecific EV uptake but rather results from EV antigen binding to the CAR on the cell surface, endocytosis inhibition using Dynasore (*41*) did not affect either EV binding measured by PKH67 staining or the CAR T cell activation induced by GPC2+ EVs (fig. S3, A to C).

To determine whether the stimulatory effects of EV antigen on CAR T cells are specific to GPC2 or represent a general characteristic of other CAR target molecules in neuroblastoma, we investigated the impact of GD2+ EVs on paired GD2 CAR T cells. We generated GD2-targeting CAR T cells (Fig. 4A) and validated their specific cytotoxicity toward GD2+ neuroblastoma cell lines (fig. S4, A and B). CAR T cell binding assays after GD2 CAR exposure to $GD2^{UltraHigh/High/Low/Neg}$ EVs (Fig. 4B) isolated from GD2 isogenic cell lines (fig. S4C) showed, similarly to GPC2+ EVs, that GD2+ EVs bind GD2 CAR T cells proportionally to GD2 EV surface amount (Fig. 4C). Furthermore, GD2+ EVs robustly activated GD2 CAR T cells as shown by the increased expression of CD69 and granzyme B after exposure to GD2+ EVs but not to control $GD2^{Neg}$ EVs (Fig. 4D). The GD2+ EV:GD2 CAR T cell synapse also resulted in enhanced GD2 CAR T cell killing of the $GD2^{Low}$ neuroblastoma cell line SK-N-AS, especially at lower E:T ratios (Fig. 4E), similar to what we observed for GPC2+ EV–preincubated GPC2 CAR T cells. This interaction was again specific given that no increased cytotoxicity was observed for CD19 CAR T cells, confirming the requirement for the interaction between EV-displayed antigen and the paired CAR (fig. S4D).

Tumor-derived antigen+ EVs stimulate tumor-infiltrating CAR T cells and are necessary for in vivo therapeutic efficacy

Next, using GPC2 as a CAR target, we explored whether target antigens on TEVs also directly modulate CAR T cells in vivo. We first generated xenograft models with decreased endogenous EV secretion

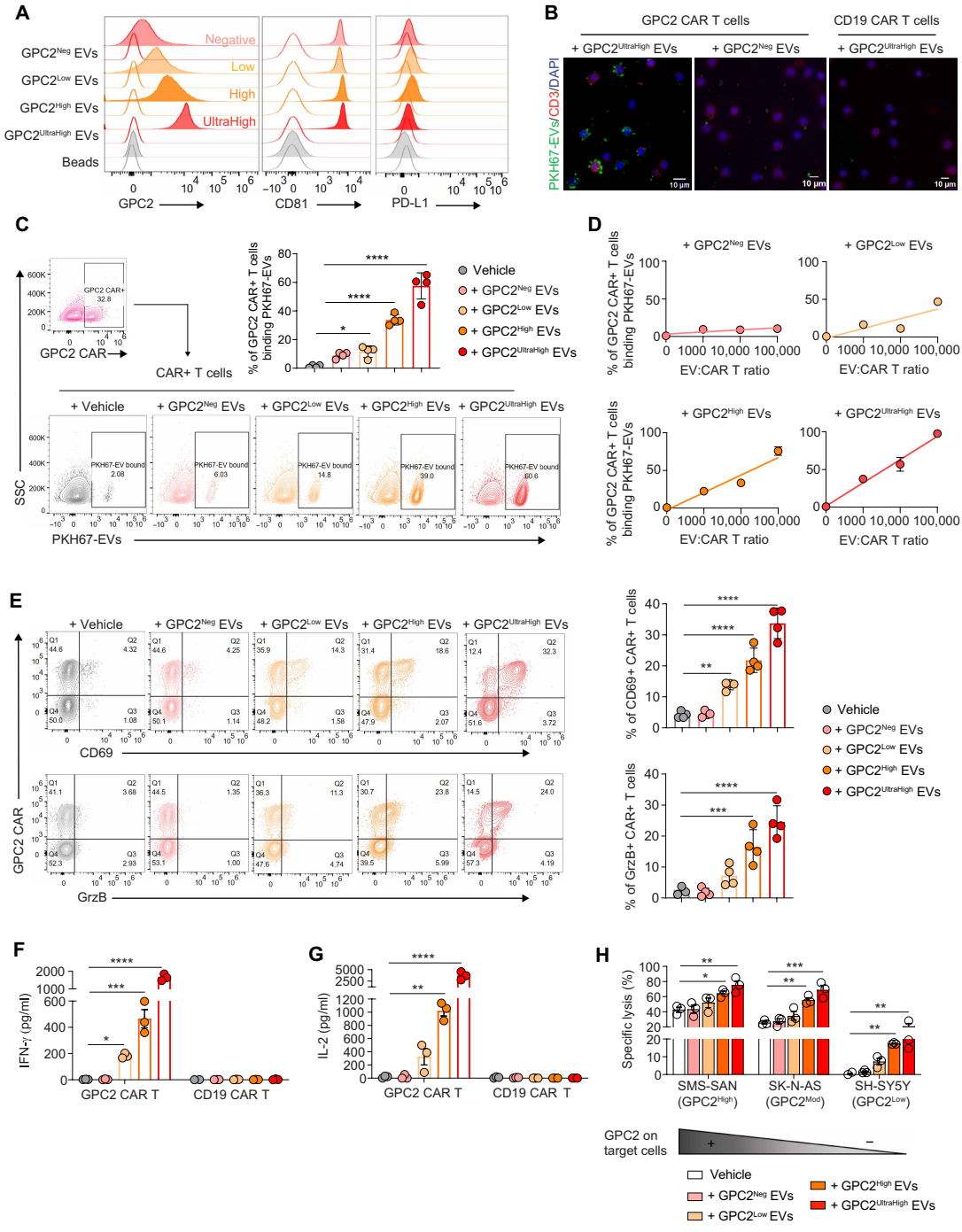

Fig. 3. GPC2+ EVs bind and activate GPC2 CAR T cells in an antigen-dependent manner enhancing T cell activation and in vitro cytotoxicity. (**A**) Representative flow cytometry histograms illustrating the abundance of GPC2, CD81 (sEV marker) and PD-L1 on EVs isolated from GPC2 isogenic cell lines. Filled colored plots represent staining with the antibody indicated on the *x* axis, and empty plots represent unstained samples. (**B**) Representative immunofluorescent images showing EV–CAR T cell binding after incubation of PKH67-labeled GPC2^{UltraHigh} EVs (green) with GPC2 CAR T cells [CD3 staining in red and 4′,6-diamidino-2-phenylindole (DAPI) in blue; left] but not CD19 CAR T cells (right). GPC2^{Neg} EVs showed no binding to CAR T cells (middle). CD3 and DAPI staining used to label T cells. Scale bars, 10 μm. (**C**) Flow cytometric gating strategy to detect EV–CAR T cell binding after incubation of PKH67-labeled GPC2+ EVs with GPC2 CAR T cells at a 10,000:1 EV:CAR+ T cell ratio. Bar chart shows the percentage of PKH67-positive GPC2 CAR+ T cells. (**D**) Percentages of PKH67-labeled GPC2$^{Neg/Low/High/UltraHigh}$ EV-bound GPC2 CAR T cells at different EV:CAR+ T cell ratios. (**E**) CAR T cell activation evaluated by CD69 (top) or granzyme B (GrzB; bottom) positivity by flow cytometry after a 16-hour incubation with GPC2$^{Neg/Low/High/UltraHigh}$ EVs. (**F** and **G**) Concentrations of IFN-γ (F) and IL-2 (G) by enzyme-linked immunosorbent assay after a 24-hour coincubation of CAR T cells with GPC2+ EVs. (**H**) EV-primed CAR T cell killing of luciferase-neuroblastoma cell lines at an E:T ratio of 1:1 after a 24-hour coincubation. Data are shown as means ± SEM. Dots represent independent biological replicates. Statistical analysis was performed using a one-way ANOVA with Dunnett's multiple comparisons test. *$P < 0.05$; **$P < 0.01$; ***$P < 0.001$; ****$P < 0.0001$. E:T, effector-to-target cell ratio.

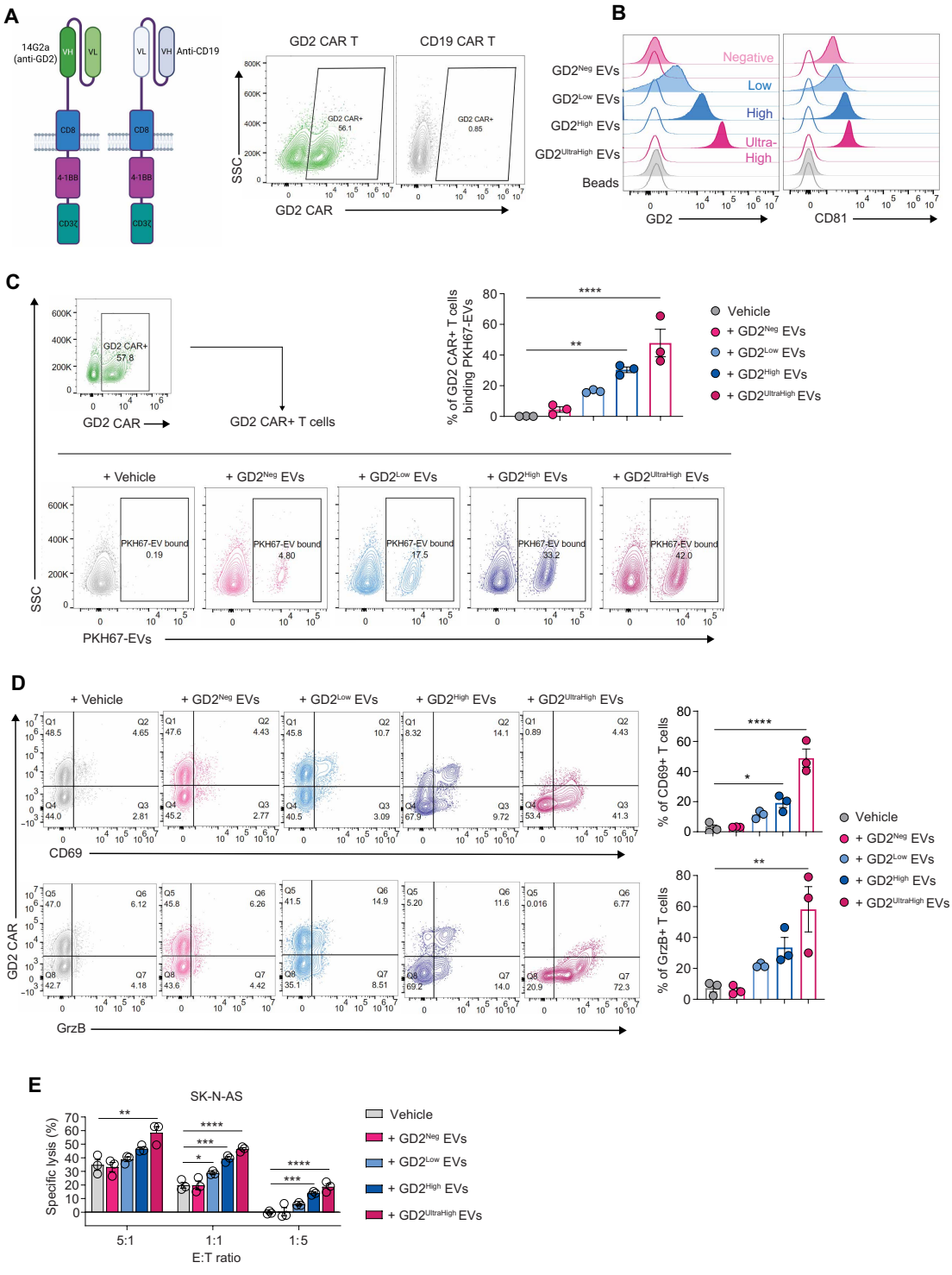

Fig. 4. GD2+ EVs bind and activate GD2-targeting CAR T cells in an antigen-dependent manner, enhancing T cell activation and in vitro cytotoxicity. (**A**) Left: Schematic illustration of CAR design, created with BioRender.com. Right: Representative transduction efficiency of GD2 and CD19 (nontargeting control) CAR T cells by flow cytometry. (**B**) Representative flow cytometry histograms illustrating the abundance of GD2 and CD81 (sEV marker) on EVs isolated from GD2 isogenic cell lines. Filled colored plots represent staining with the antibody indicated on the *x* axis, and empty plots represent unstained samples. (**C**) Flow cytometric gating strategy to detect EV–CAR T cell binding after incubation of PKH67-labeled GD2+ EVs with GD2 CAR T cells at a 10,000:1 EV:CAR+ T cell ratio. Bar chart shows the percentage of PKH67-positive GD2 CAR+ T cells. (**D**) Flow cytometric gating strategy to detect CD69 (top) and granzyme B (GrzB; bottom) positivity on GD2 CAR T cells after a 16-hour coincubation with GD2+ EVs. The bar charts show the percentage of CD69- or GrzB-positive T cells. (**E**) EV-primed CAR T cell lysis of luciferase–SK-N-AS cells at different E:T ratios after a 24-hour coincubation. Data are shown as means ± SEM. Dots represent independent biological replicates. Statistical analysis was performed using a one-way ANOVA with Dunnett's multiple comparisons test. **P* < 0.05; ***P* < 0.01; ****P* < 0.001; *****P* < 0.0001.

by CRISPR-Cas9 knockout (KO) of *RAB27A*, an essential GTPase (guanosine triphosphatase) involved in EV release (*42*). RAB27A KO was efficiently achieved in neuroblastoma cell lines with two unique guide RNAs (Fig. 5A and fig. S5A). As expected, loss of RAB27A markedly suppressed TEV secretion both in vitro (Fig. 5B and fig. S5B) and in vivo after subcutaneous injection into NSG mice (Fig. 5C), without modulating the cell surface expression of GPC2 (fig. S5C). However, despite only modest differences in cell proliferation in vitro compared with wild-type (WT) cells (fig. S5D), RAB27A KO cells grew substantially slower in vivo compared with WT xenografts (fig. S5E), preventing us from directly comparing CAR T cell response between the RAB27A KO and WT models and suggesting a potential role for EVs in neuroblastoma in vivo tumor growth. Alternatively, we used the SK-N-AS RAB27A KO xenograft—a model with depleted TEV secretion and low GPC2 expression—to compare GPC2 CAR T cell efficacy with and without exogenous intratumor administration of $GPC2^{High}$ TEVs, isolated from SK-N-AS–GPC2 isogenic cells. (Fig. 5D). Here, we observed that injection of $GPC2^{High}$ TEVs significantly enhanced the efficacy of coinfused GPC2 CAR T cells against $GPC2^{low}$ SK-N-AS xenografts, as demonstrated by the difference in tumor growth (Fig. 5, E and F, and fig. S5F) and the modestly prolonged survival of tumor-bearing mice in the $GPC2^{High}$ TEV cohort (Fig. 5G). $GPC2^{Low}$ TEVs isolated from paired-WT SK-N-AS cells had minimal effect on CAR T efficacy, further confirming that the superior CAR T efficacy was specifically induced by the presence of GPC2 on coinfused TEVs (fig. S5G). Furthermore, we analyzed satellite tumors 7 days after GPC2 CAR T cell administration to quantify CAR T cell infiltration, activation, and phenotype. Consistent with the observed enhanced antitumor response, the exogenous administration of $GPC2^{High}$ TEVs resulted in significantly enhanced tumor infiltration of both total and activated (CD69+ CD25+) GPC2 CAR T cells (Fig. 5, H and I) with an increased effector memory (EM) phenotype (fig. S5H) but with no differences in expression of T cell exhaustion markers (PD-1 and LAG3) compared to GPC2 CAR T cells alone (fig. S5I; gating strategy in fig. S6A).

To further validate these findings in an orthogonal EV-depleted in vivo model, we next evaluated GPC2 CAR T cell efficacy in a $GPC2^{High}$ neuroblastoma xenograft (isogenic SK-N-AS–GPC2 tumors), achieving exogenous EV inhibition with the neutral sphingomyelinase inhibitor GW4869 (*43*). We first demonstrated that daily treatment with GW4869 (1.25 mg/kg) induced a stable decrease in EV secretion (Fig. 5J), without modulating in vivo tumor growth kinetics or GPC2 cell surface density (fig. S6, B and C). Here, we treated isogenic SK-N-AS–GPC2 xenografts with a subtherapeutic dose of GPC2 CAR T cells (1 million GPC2 CAR+ T cells; 10% of typical dose) concurrently with the EV-inhibiting drug GW4869 (Fig. 5K). Pharmacologic inhibition of GPC2+ EV tumor secretion significantly decreased CAR T cell efficacy, which could be rescued by intratumoral injection of $GPC2^{High}$ TEVs (Fig. 5, L to N). Analysis of satellite tumors 7 days after GPC2 CAR T cell infusion validated a direct effect of TEVs on tumor-infiltrating CAR T cells given that we also observed an increase in both total and activated (CD69+ CD25+) GPC2 CAR T cells with a more prevalent EM phenotype in tumors that had GPC2+ EVs present (either those that received vehicle or where EV inhibition was rescued by intratumoral administration of $GPC2^{High}$ TEVs; Fig. 5, O and P, and fig. S6D). Collectively, these studies demonstrate that the in vivo availability of antigen-exposing TEVs facilitates CAR T cell tumor homing, activation, and antitumor efficacy.

Engineering target antigen–displaying SyntEVs with albumin or GD2 binding properties further enhances GPC2 CAR T cell in vivo persistence and antitumor efficacy

We next looked to further capitalize on the importance of GPC2+ EVs to GPC2 CAR T cell activation and enhanced antitumor efficacy by testing whether intravenously administered GPC2+ EVs might serve to serially stimulate GPC2 CAR T cells either peripherally or in the TME using different engineering strategies. For this therapeutic purpose, we chose genetically modified HEK293T cells as producer cells for nontumor GPC2+ EV isolation (Fig. 6A), herein referred to as SyntEVs to distinguish them from previously described GPC2+ TEVs. We first used MS to characterize these SyntEVs and confirmed high abundance of GPC2 and low amounts of some inhibitory checkpoint ligands (PD-L1 and PVR). Other immunomodulatory proteins were undetectable such as the programmed cell death ligand 2 (PD-L2), fibrinogen like 1 (FGL1), herpesvirus entry mediator (HVEM), v-set and immunoglobulin domain containing protein 3 (VSIG3), and galectin 9 proteins (fig. S7, A and B). To better understand the optimal localization for GPC2+ EVs to reside to most effectively prime GPC2 CAR T cells in vivo, we engineered our nontumor GPC2+ SyntEVs to bind either serum albumin (ALB) to enhance their circulation half-life or the neuroblastoma-associated antigen GD2 to enhance their tumor infiltration (Fig. 6A). First, to achieve EV binding to albumin, we exploited two well-characterized engineered albumin-binding domains (ABDs) with affinity to both human and murine albumin (ABD035 and ABD094) (*44*, *45*), which were inserted into the extracellular loops of the tetraspanin CD9 (*46*). CD9 was either engineered with ABDs in both loops (×2), or with a single ABD in the second loop (L2), for a total of four unique anti–ALB-CD9 combinations (fig. S7C). Alternatively, GD2 binding was achieved by expression of a recombinant receptor including the anti-GD2 scFv 14G2a, followed by PDGFR transmembrane and intracellular domains (Fig. 6A). A CD81–green fluorescent protein (GFP) fusion protein was also expressed in the EV producer HEK293T cells to achieve production of GFP+ EVs (Fig. 6A). The expression of the transgenes in the producer cells, as well as the binding properties of the corresponding isolated EVs, was verified by flow cytometry (fig. S7, D and E). Among the four different iterations of anti–ALB-CD9, we selected the one with the highest binding to albumin as quantified by flow cytometry (CD9-ABD094-L2; fig. S7D). The affinity of the isolated GPC2+ anti-ALB SyntEVs for both murine and human albumin, as well as the affinity of the GPC2+ anti-GD2 EVs for the 1A7 anti-idiotype antibody specific for the 14G2a binder, was also validated (Fig. 6B, top). Comparable amounts of GPC2 exposure and GFP positivity were observed among the different engineered EVs (Fig. 6B, bottom).

Next, we performed EV-GPC2 CAR T cell coincubation studies to verify binding to GPC2 CAR T cells by flow cytometry leveraging the intrinsic fluorescence of the EVs provided by GFP. As expected, on the basis of the similar GPC2 densities, all the GPC2+ engineered SyntEVs (GPC2+, GPC2+ anti-ALB, and GPC2+ anti-GD2) exhibited comparable GPC2 CAR T cell binding (63.4% ± 7.1), whereas only minimal binding was observed with the $GPC2^{Neg}$ GFP+ control EVs, suggesting that the interaction is driven by direct CAR engagement with EV-displayed GPC2 (Fig. 6, C and D). Accordingly, comparable GPC2 CAR T cell activation was induced by GPC2+ engineered SyntEVs, as shown by CD69 and granzyme B expression in the CAR+ T cell subset (Fig. 6, E and F). Conversely,

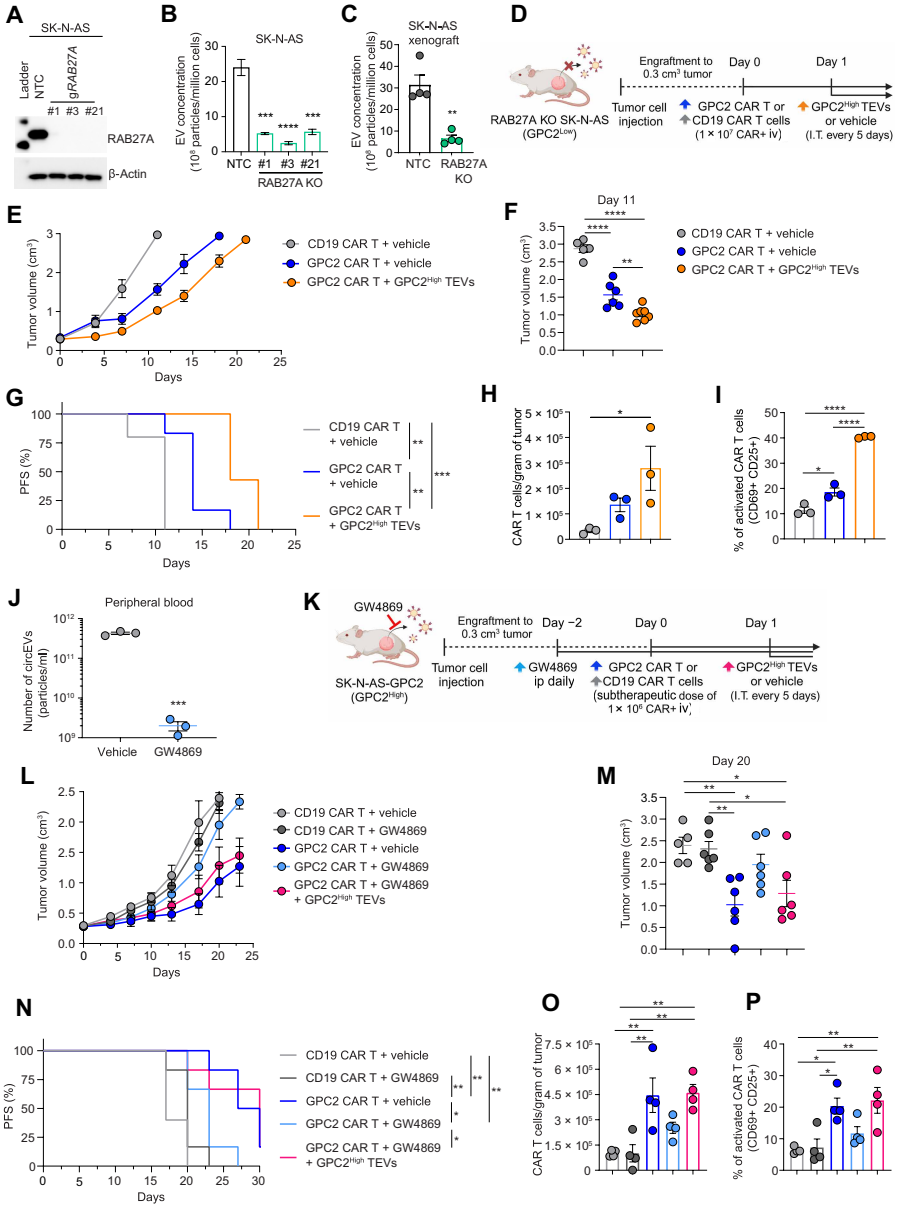

Fig. 5. Tumor-derived GPC2+ EVs stimulate tumor-infiltrating CAR T cells and are necessary for in vivo antitumor efficacy. (**A**) RAB27A Western blot of nontargeting control (NTC) and three RAB27A KO SK-N-AS clones. β-Actin served as a loading control. (**B**) EV counts from the supernatant of control NTC and three RAB27A KO SK-N-AS clones quantified by NTA. (**C**) In vivo TEV secretion by RAB27A KO compared with NTC SK-N-AS xenografts by NTA. TEVs were isolated from tumors collected on day 20 after engraftment in SCID mice. (**D**) Experimental design of in vivo study using the SK-N-AS RAB27A KO xenograft ($GPC2^{Low}$) to compare GPC2 CAR T cell efficacy with and without exogenous intratumoral administration of $GPC2^{High}$ TEVs from SK-N-AS–GPC2 cells. (**E**) SK-N-AS RAB27A KO tumor growth curves measured serially with calipers after treatment with nontargeting control CD19 or GPC2 CAR T cells coadministered with intratumorally injected $GPC2^{High}$ TEVs or vehicle ($n = 5$ to 7 mice per group). (**F**) Tumor volumes at day 11 after CAR T cell administration for treatment groups in (E). (**G**) Progression-free survival (PFS) for the different CAR treatment cohorts shown in (E) and (F). (**H**) Quantification of tumor-infiltrating human CD45+ (CAR T) cells by flow cytometry from satellite tumors treated according to D ($n = 3$ tumors per group, day 7). (**I**) Quantification of activated (CD69+ CD25+) CAR T cells gated on human CD45+ cells in (H). (**J**) Number of circEVs from SCID mice bearing SK-N-AS–GPC2 tumors treated daily with GW4869 (1.25 mg/kg, intraperitoneally) or vehicle. Treatment started when tumors reached a volume of ~0.2 cm^3, and circEVs were collected from the peripheral blood after 10 days. (**K**) In vivo study design testing the efficacy of a subtherapeutic dose of GPC2 CAR T cells (1×10^6 CAR+ cells) on SK-N-AS–GPC2 xenograft ($GPC2^{High}$) growth when given concurrently with GW4869 with or without intratumoral rescue with $GPC2^{High}$ TEVs from SK-N-AS–GPC2 cells. (**L**) SK-N-AS–GPC2 tumor growth curves after treatment with nontargeting control CD19 or GPC2 CAR T cells coadministered with GW4869 or vehicle with or without intratumorally injected $GPC2^{High}$ TEVs ($n = 5$ or 6 mice per group). (**M**) Tumor volumes at day 20 after CAR T cell administration for treatment groups in (L). (**N**) PFS for CAR treatment cohorts shown in (L) and (M). (**O**) Quantification of tumor-infiltrating human CD45+ (CAR T) cells by flow cytometry from satellite tumors ($n = 4$ tumors per group) treated according to (K). Tumor samples were collected at day 7 after CAR T cell injection. (**P**) Quantification of activated (CD69+ CD25+) CAR T cells gated on human CD45+ cells in (O). Data are shown as means ± SEM. Dots represent independent biological replicates. Statistical analysis was performed using the log-rank test for PFS curves or a one-way ANOVA with Tukey's multiple comparisons test [(B), (F), (H), (I), (M), (O), and (P)] or Mann-Whitney test [(C) and (J)] to evaluate differences between groups. *$P < 0.05$; **$P < 0.01$; ***$P < 0.001$; ****$P < 0.0001$. Illustrations in (D) and (K) created with BioRender.com. KO, knockout; iv, intravenously; I.T., intratumorally; ip, intraperitoneally.

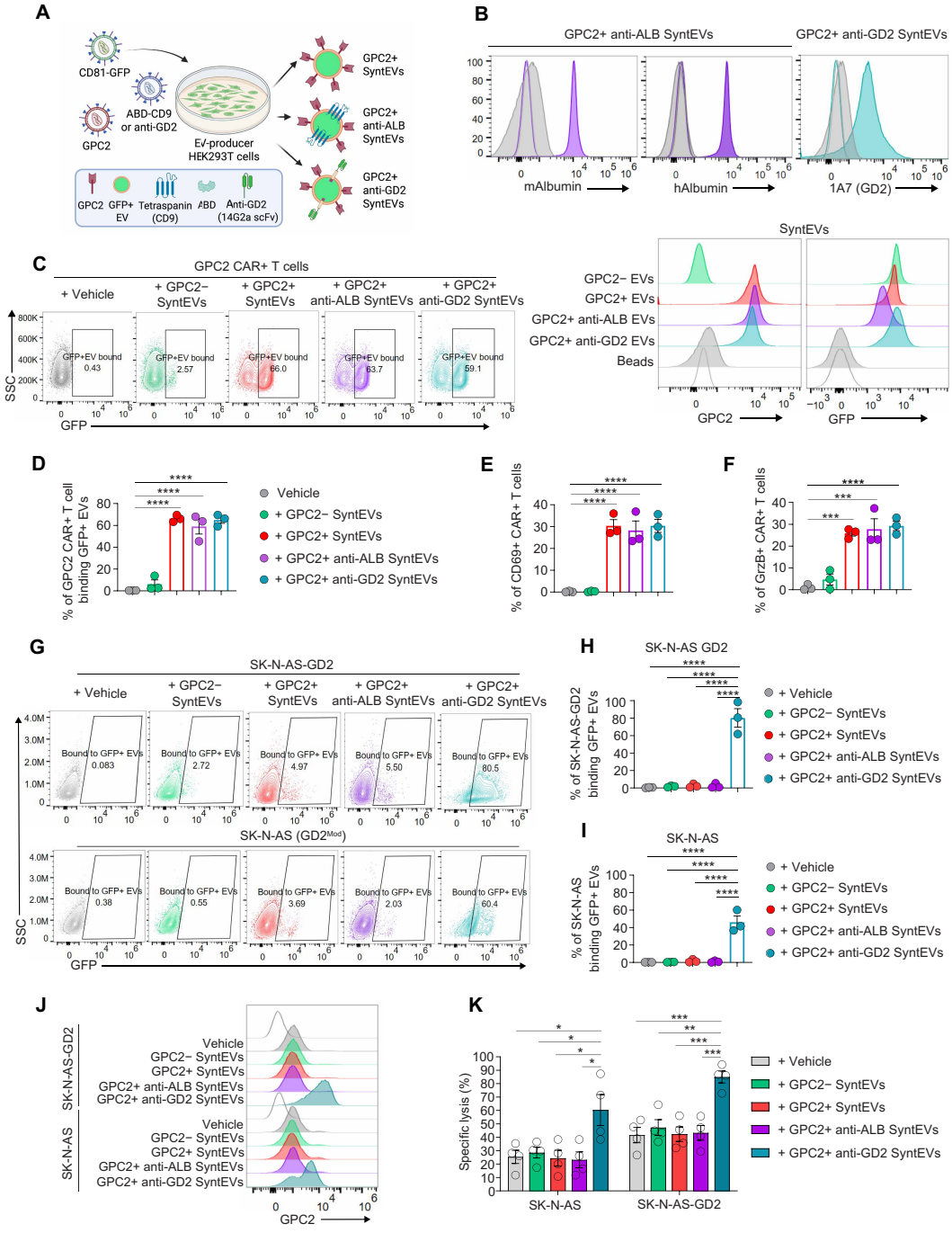

Fig. 6. Engineering GPC2+ SyntEVs with albumin- or GD2-binding properties as CAR T cell engagers. (**A**) Schematic illustration showing the design of GPC2+ SyntEVs (GPC2+, GPC2+ anti-ALB, and GPC2+ anti-GD2) derived from HEK293T cells stably engineered with lentiviral transduction. Figure created with BioRender.com. (**B**) Top: Representative flow cytometry histograms showing GPC2+ anti-ALB SyntEV binding to murine (m) and human (h) serum albumin (purple) and GPC2+ anti-GD2 EV binding to the 1A7 anti-idiotype antibody specific for 14G2a (cyan). Bottom: Flow cytometry histograms showing the GPC2 cell surface expression and GFP signal in GPC2+ ± anti-ALB/GD2 SyntEVs and GPC2− GFP+ control EVs. Stained beads without EVs are shown as gray filled plots, whereas empty plots represent unstained beads. (**C**) Representative flow cytometry plots for EV–CAR T cell binding after incubation of GFP+ GPC2− (control) or GPC2+ ± anti-ALB/GD2 SyntEVs with GPC2 CAR T cells at a 10,000:1 EV:CAR+ T cell ratio. (**D**) Quantification of EV-bound GPC2 CAR T cells from (C). (**E** and **F**) CAR T cell activation evaluated by CD69 (E) or granzyme B [GrzB (F)] by flow cytometry after a 24-hour coincubation with GPC2+ ± anti-ALB/GD2 SyntEVs or vehicle. (**G**) Representative flow cytometry plots for EV–neuroblastoma cell binding after incubation of SK-N-AS–GD2 (top) or SK-N-AS (bottom) cells with GFP+ GPC2+ ± anti-ALB/GD2 SyntEVs at a 10,000:1 EV:tumor cell ratio. (**H** and **I**) Quantification of EV-bound SK-N-AS–GD2 (H) or SK-N-AS (I) cells from (G). (**J**) GPC2 abundance on SK-N-AS–GD2 or SK-N-AS cells from (G) to (I). (**K**) GPC2 CAR T cell lysis of luciferase–SK-N-AS–GD2 or luciferase–SK-N-AS cells after preincubation with GPC2+ ± anti-ALB/GD2 SyntEVs or vehicle for 1 hour. Data are shown as means ± SEM. Dots represent independent biological replicates. Statistical analysis was performed using a one-way ANOVA with Dunnett's multiple comparisons test [(D), (E), and (F)] or a one-way ANOVA with Tukey's multiple comparisons test [(H), (I), and (K)]. *$P < 0.05$; **$P < 0.01$; ***$P < 0.001$; ****$P < 0.0001$. Mod, moderate.

no activation was observed in GPC2 CAR T cells after incubation with the $GPC2^{Neg}$ GFP+ EVs (Fig. 6, E and F) or in CD19 CAR T cells after exposure to GPC2+ SyntEVs (fig. S7F). To further define the activation profile of GPC2 CAR T cells upon interaction with the engineered GPC2+ SyntEVs, we performed single-cell functional cytokine immune profiling. This analysis revealed increased expression of not only effector cytokines, such as IFN-γ, but also elevation of stimulatory (IL-2 and granulocyte-macrophage colony-stimulating factor) and chemoattractive [macrophage inflammatory protein 1β (MIP-1β)] cytokines compared with GPC2 CAR T cells exposed to $GPC2^{Neg}$ EVs (fig. S7, G and H).

We also tested the ability of our GPC2+ GD2-binding SyntEVs to specifically bind GD2+ neuroblastoma cells and potentially deliver extra GPC2 antigen to tumor cells. Using flow assays, we compared the percentages of EV-bound neuroblastoma cells after coincubation with different GPC2+ SyntEVs. Binding, detected as GFP positivity, was observed exclusively in GD2+ cell lines exposed to GD2-binding SyntEVs and correlated with the GD2 abundance on the target cell surface (SK-N-AS–GD2 > SK-N-AS >>> HEK293T; Fig. 6, G to I and fig. S8, A to C). Furthermore, GD2-mediated EV–tumor cell coating increased GPC2 cell surface expression in SK-N-AS and SK-N-AS–GD2 (Fig. 6J) but not in control HEK293T (fig. S8D) cells. Last, this higher GPC2 cell surface density induced by EV binding also resulted in selectively and potently increasing susceptibility to GPC2 CAR T cell–mediated cytotoxicity (Fig. 6K and fig. S8E).

Next, to determine whether the GPC2+ ALB-binding SyntEVs can be better detected in the peripheral blood of mice and to validate tumor trafficking of the GPC2+ anti-GD2 SyntEVs, we intravenously injected NSG mice bearing SK-N-AS–GD2 xenografts with two doses of each type of engineered SyntEV (GPC2+, GPC2+ anti-ALB, or GPC2+ anti-GD2; on days 1 and 3) and collected peripheral blood and tumor 5 hours after the second EV administration. As predicted, the GFP signal evaluated by Western blot of peripheral blood–isolated circEVs and tumor lysates showed enhanced detectability of GPC2+ anti-ALB SyntEVs in the peripheral blood and more robust tumor trafficking for the GPC2+ anti-GD2 SyntEVs (Fig. 7A). Next, to understand whether these engineered GPC2+ SyntEV variants may better enhance GPC2 CAR T cell efficacy in vivo, we serially intravenously infused them in combination with GPC2 CAR T cells in NSG mice bearing SK-N-AS–GD2 ($GPC2^{Low}$, $GD2^{High}$) cell line xenografts (Fig. 7B and fig. S9A). All GPC2+ SyntEVs variants resulted in significantly better tumor control than GPC2 CAR T cells alone (Fig. 7C and fig. S9, B and C). However, the ALB and GD2-binding GPC2+ SyntEVs outperformed the unmodified GPC2+ SyntEVs, preventing overt tumor relapse and enabling survival until day 80 after CAR T cell administration, when the study was concluded because most mice acquired xenogeneic graft-versus-host disease (xGvHD; Fig. 7D), an expected outcome due to human T cell reactivity toward host murine tissues (*47*). All EV administrations were well tolerated given that no signs of systemic toxicity or changes in body weight were observed, except the late weight loss associated with xGvHD onset (fig. S9D). The differences in antitumor response were associated with increased persistence of GPC2 CAR T cells in the peripheral blood of mice receiving GPC2+ SyntEVs, with the highest peripheral human T cell count detected in the anti-ALB SyntEV treatment group 20 days after CAR T cell infusion (Fig. 7E). Tumor infiltration of GPC2 CAR T cells in the presence or absence of coadministration of GPC2+ SyntEVs was also verified by human CD3 immunohistochemistry (IHC) in satellite tumors collected 10 days after CAR T cell injection (fig. S10, A to D).

To further validate the therapeutic relevance of antigen-displaying EVs on CAR T cell efficacy in neuroblastoma, GPC2+ anti-ALB or anti-GD2 EVs were next tested in the human neuroblastoma PDX model, COG-N-561x, which exhibits both high cell surface GPC2 and GD2. A previous study from our laboratory showed that GPC2 CAR T cells can induce initial complete tumor regressions in this neuroblastoma PDX but that tumor relapses occur ~2.5 weeks after CAR T cell injection (*19*). Thus, this study was specifically designed to evaluate the ability of GPC2+ EVs to reinvigorate CAR T cells through EV-induced antigen stimulation after this initial tumor eradication. After CAR T cell injection, mice were monitored for tumor volume and peripheral CAR T cell counts. On day 17 (week 2.5), when the T cell count in the peripheral blood dropped below 200 cells/μl, GPC2+ EV administration was initiated (Fig. 7F). Infusion of both anti-ALB and anti-GD2 GPC2+ EVs resulted in substantial peripheral CAR T cell expansion (Fig. 7G), prolonged animal survival (Fig. 7H), and enhanced tumor control compared with GPC2 CAR T cells alone (Fig. 7I and fig. S11A), without signs of toxicity (fig. S11B). Last, nine additional mice were also treated with CAR T cells when tumor volume reached a size of 0.3 ± 0.05 cm^3, followed by administration of GPC2+ GD2-binding EVs or vehicle, according to the same in vivo study design. IHC and flow cytometry analysis of tumors collected on day 20, 5 hours after the second EV dose, confirmed that GPC2 was down-regulated in tumors treated with GPC2 CAR T cells (Fig. 7J and fig. S11C). In contrast, tumors from mice vaccinated with GPC2+ GD2-binding EVs exhibited increased GPC2 expression (Fig. 7J and fig. S11C) and also had a significant enhancement in human T cell recruitment (Fig. 7K), demonstrating the engineered EVs' ability to traffic to the tumor, supplement the tumor with extra GPC2 antigen, and enhance GPC2 CAR T cell homing.

DISCUSSION

Antigen heterogeneity, limited tumor infiltration, and poor persistence of adoptively transferred T cells are major barriers limiting the durable efficacy of CAR T cell therapy in solid tumors (*48*), including the commonly lethal embryonal malignancy neuroblastoma. To overcome these challenges, it is essential to understand the molecular mechanisms regulating CAR T cell response, including the role of TEVs as intercellular messengers between tumor and immune cells. Here, we demonstrate that GPC2+ and GD2+ EVs can be specifically detected in the peripheral blood of mice bearing neuroblastoma PDXs, where the degree of GPC2 and GD2 positivity correlates both with tumor size and tumor antigen expression. GPC2 and GD2 were also selectively detected on circEVs isolated from plasma of patients with neuroblastoma, suggesting that they may also be useful diagnostically in the pediatric oncology clinic. Other glypicans have been previously identified on circEVs from patients with cancer, highlighted by GPC3 in hepatocellular carcinoma (*39*) and GPC1 in pancreatic cancer (*38*), where GPC1+ circEVs distinguished healthy participants and patients with benign pancreatic disease from those with overt pancreatic cancer. Although our analyses are limited to a discovery cohort and will require further validation in a larger

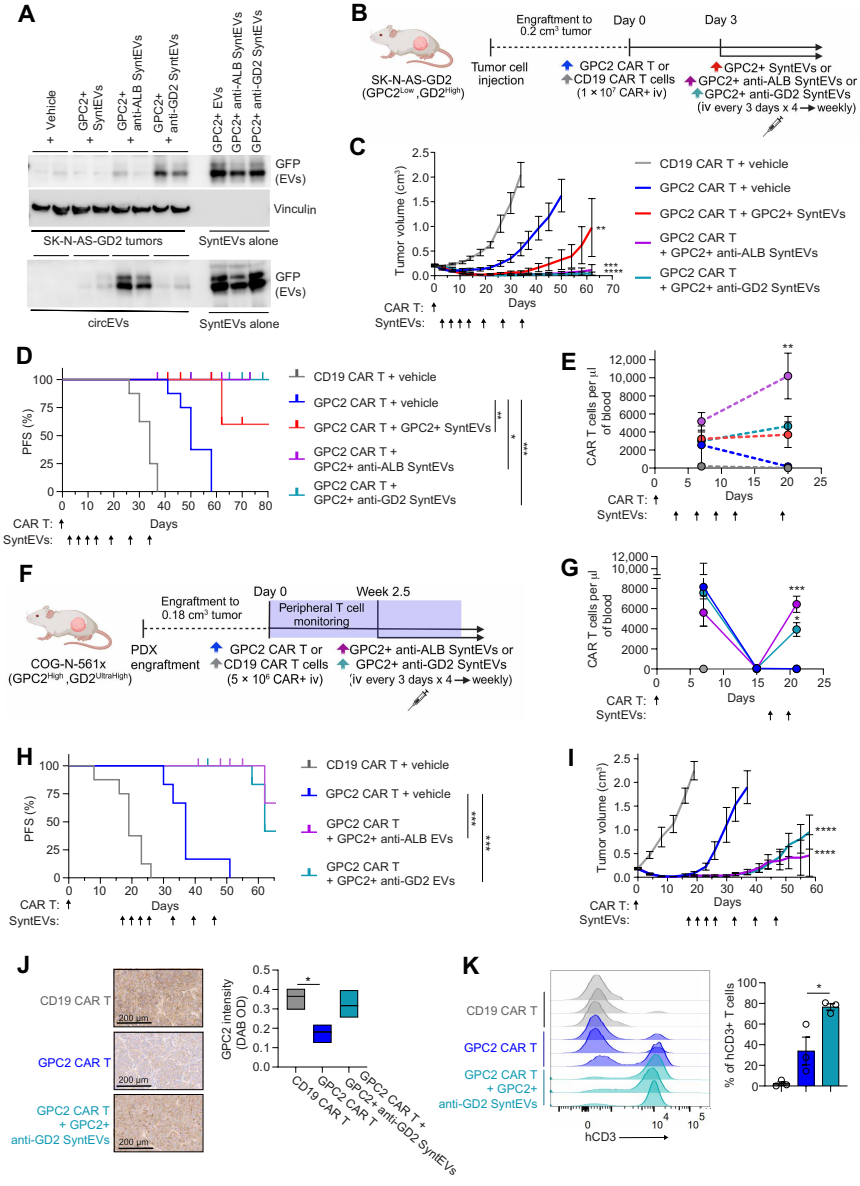

Fig. 7. Armored GPC2+ SyntEVs boost GPC2 CAR T cell in vivo persistence and antitumor efficacy. (**A**) Top: GFP Western blot of SK-N-AS–GD2 tumors from mice treated with two intravenous doses of GPC2+ SyntEVs 5 hours after the last EV administration. Bottom: GFP Western blot of circEVs isolated from the peripheral blood of the same mice. Respective purified SyntEV controls are also shown to validate similar levels of GFP in each EV cohort. (**B**) Experimental design of in vivo study testing GPC2 CAR T cells in combination with GPC2+ EVs in SK-N-AS–GD2 xenografts ($GPC2^{Low}$, $GD2^{High}$). (**C**) SK-N-AS–GD2 tumor growth curves after treatment with CD19 or GPC2 CAR T cells in combination with naked or armored GPC2+ SyntEVs ($n = 8$ or 9 mice per group). The indicated P values correspond to differences between groups at day 45. (**D**) PFS for the different CAR treatment cohorts shown in (B) and (C). (**E**) Quantification of circulating hCD45+ hCD3+ (CAR T) cells by flow cytometry in peripheral blood samples from mice enrolled on study shown in (B) to (D) ($n = 4$ mice per group). Samples were collected at day 7 (after two EV doses) and day 20 (after five EV doses) after CAR T cell infusion. (**F**) Experimental design of in vivo study testing GPC2 CAR T cell vaccination with GPC2+ ± anti-ALB/GD2 SyntEVs in the neuroblastoma COG-N-561x PDX ($GPC2^{High}$, $GD2^{UltraHigh}$) mouse model. (**G**) Quantification of circulating hCD45+ hCD3+ (CAR T) cells by flow cytometry from peripheral blood samples from COG-N-561x–bearing mice enrolled on the study shown in (F) ($n = 3$ or 4 mice per group). Samples were collected at day 7 and 14 (before EV administration) and day 21 (after two EV doses) after CAR T cell injection. Only one mouse remained in the control CD19 CAR group at day 21. (**H**) PFS for COG-N-561x–bearing mice after treatment with CD19 or GPC2 CAR T cells in combination with naked or armored GPC2+ SyntEVs as shown in (F). (**I**) COG-N-561x tumor growth curves for the different CAR treatment cohorts shown in (F) to (H). Statistical analysis was performed by comparing tumor volumes at day 37. (**J**) GPC2 IHC on satellite COG-N-561x tumors 20 days posttreatment with CD19 or GPC2 CAR T cells with or without GPC2+ anti-GD2 SyntEVs according to (F). A representative tumor (left) and GPC2 IHC staining intensity quantification for all tumors ($n = 3$ per group; right) are shown. Scale bars, 200 µm. (**K**) Quantification of human T cells by flow cytometry in COG-N-561x tumors shown in (J) (20 days after CAR T cell infusion). Flow cytometry plots showing CD3 staining (left) and T cell quantification as % of hCD3+ cells (right) are shown ($n = 3$ per group). Data are shown as means ± SEM. Dots represent independent biological replicates. Statistical analysis was performed using the log-rank test for PFS curves or a one-way ANOVA with Tukey's [(C), (E), (G), and (I)] or Dunnett's [(J) and (K)] multiple comparisons test to evaluate differences between groups. *$P < 0.05$; **$P < 0.01$; ***$P < 0.001$; ****$P < 0.0001$. Dotted lines in (E) indicate CAR T cell count from unpaired peripheral blood samples, whereas solid lines in (G) represent CAR T cell count from paired peripheral blood samples. Illustrations in (B) and (F) created with BioRender.com. OD, optical density.

independent patient series, these proof-of-concept studies support further exploring circEVs as a potential noninvasive tumor biomarker for children with neuroblastoma and potentially other lethal GPC2+ malignancies. For example, much like circulating tumor DNA profiling might offer clinically relevant real-time information on targetable genomic alterations for children with neuroblastoma (*49*), serial protein profiling of circEVs might provide data to determine eligibility for personalized cell surface–targeted immunotherapies. Furthermore, our results showing the functional effects of TEV-exposed target antigen on CAR T cells also suggest that the abundance of circEVs should potentially be taken into account when administrating immunotherapies. Correlative research studies monitoring EV kinetics pre- and posttherapy should be incorporated into ongoing CAR T cell trials, similar to currently active clinical trials monitoring the kinetics of circEVs during combination therapies using immune checkpoint inhibitors in patients with high-grade glioma (NCT03576612) or melanoma (NCT04581382). Considering that GPC2, GD2, and other tumor antigens (such as B7-H3 and L1CAM) exposed on the TEV surface are targets for clinically available CAR T cells (*23*), these data are immediately relevant to several ongoing clinical trials.

Prior studies in hematological malignancies have dissected the interaction between TEVs and CD19 targeting CAR T cells, showing that TEVs carrying both target antigen and the inhibitory checkpoint protein PD-L1 inhibit CD19 CAR T cells (*50*). Similarly, a recent study in pancreatic cancer showed inhibitory effects of TEVs on mesothelin-redirected CAR T cells (*14*). Zhong *et al.* elegantly demonstrated that, although target antigen on TEVs is essential to induce the synapse of TEV and CAR, high abundance of PD-L1 on TEVs ultimately induces mesothelin CAR T inhibition. Conversely, our studies showed that target antigen exposed on neuroblastoma-derived TEVs enhances the effectiveness of paired CAR T cells. This discrepancy with previous studies may be attributed to differences in the other protein cargo components of neuroblastoma-derived EVs, especially the limited expression of PD-L1 (*51*). Even after IFN-γ stimulation, resembling a condition occurring in the TME in the presence of an effective CAR T cell response (*52*), PD-L1 upregulation on neuroblastoma TEVs was minimal when compared with even the basal exposure on melanoma-derived EVs. Because of the specific cargo of neuroblastoma TEVs, we focused on defining the effects of target antigen exposure on EVs on CAR T cell functionality. However, TEV cargo composition appears to be cancer specific (*53*), and the effects of tumor antigens loaded on TEVs may vary across tumor types on the basis of other coexposed molecules, particularly immune inhibitory checkpoint or costimulatory molecules (*5*, *6*).

In addition to being natural nanocarriers (*53*), EVs can also be engineered to therapeutically deliver functional molecules specifically to tumors, thus offering potential as next-generation targeted nanomedicines (*54*, *55*). For example, genetically engineered EVs, called SMART-Exos, with surface display of anti-human CD3 and anti-human HER2 antibodies, have shown preclinical antitumor efficacy by redirecting cytotoxic T cells toward HER2-expressing breast cancer cells (*56*). In support of an immunotherapeutic application of EVs, CAR EVs derived from effector CAR T cells have been nominated as an "off-the-shelf therapeutic" with lower risk of toxicities, such as cytokine release syndrome (CRS), compared with respective CAR T cell treatments (*57*). Clinically, vaccination strategies based on antigen-loaded DC-derived EVs are also currently being explored (NCT01159288). These studies collectively underscore the potential value of engineered EVs in the clinic. Here, we further extend the therapeutic potential of EVs by exploring antigen-displaying EVs as a CAR T cell vaccination strategy in preclinical solid tumor models. Despite finding minimal PD-L1 exposure on neuroblastoma TEVs, to avoid any potential immune-inhibitory effects commonly associated with TEVs (*5*, *14*), we opted to use non-tumor EVs engineered to display the antigen of interest, GPC2, for these purposes (herein referred to as GPC2+ SyntEVs). We confirmed with MS studies that these GPC2+ SyntEVs lack common inhibitory checkpoint molecules, such as PD-L1 and PVR, in their protein cargo.

The importance of long-term CAR T cell persistence for durable clinical efficacy has been delineated for several cancers (*58*). However, CAR T cell levels typically decline rapidly after infusion in patients with solid tumors (*59*, *60*), in part because of the impaired accessibility of adoptively transferred cells to target cells within solid lesions and the absence of additional costimulation signals upon target encounter in the hostile immunosuppressive TME. In contrast, CAR T cells targeting hematologic malignancies immediately encounter their targets on circulating cells upon entering the bloodstream, a factor that may contribute substantially to their sustained antitumor responses. To address these limitations, lipid nanoparticles delivering antigen-encoding RNAs (*61*) and amphiphile CAR ligands targeting lymph nodes through antigen-linking to albumin-binding phospholipid polymers (*62*) have been used to boost solid tumor CAR T cell responses. Both methods promote priming and expansion of CAR T cells outside the immunosuppressive TME (*61*, *62*). Here, we explored an alternative approach to address the lack of effective extratumoral CAR stimulation in solid tumors, using GPC2+ SyntEVs to boost GPC2 CAR T cells. Although we saw enhanced in vivo GPC2 CAR T cell efficacy when given in combination with serial dosing of GPC2+ EVs, given that exogenous EVs introduced into the circulation are known to have a short half-life ranging from 30 min to 5 hours depending on the cell source (*63*), we further hypothesized that extending the circulation half-life of our GPC2+ SyntEVs by facilitating binding to serum albumin (*46*) might further enhance their ability to positively modulate GPC2 CAR T cells. In turn, our in vivo data using these "armored" GPC2+ SyntEVs suggested that GPC2+ ALB-binding SyntEVs persisted longer in the circulation, compared with naked GPC2+ SyntEVs, and markedly enhanced GPC2 CAR T cell peripheral proliferation. Although increasing CAR T cell persistence in the periphery might lead to on-target–off-tumor toxicities or CRS, these adverse effects were not observed in mice that received these mouse/human cross-reacting GPC2 CAR T cells along with serial intravenous injections of GPC2+ ALB-binding SyntEVs. However, because development of xGvHD due to expected human CAR T cell reactivity toward host murine tissues limits the time of evaluation in this model, the long-term risks of prolonged CAR T cell stimulation from GPC2+ SyntEVs requires further investigation.

We also tested a different armored-EV strategy aimed at addressing a second major limitation to CAR T cell solid tumor efficacy—antigen down-regulation (*3*). CAR-induced tumor target down-regulation has been observed with most effective CAR T cell therapies, including GPC2 CARs (*21*) and CARs targeting CD19 (*64*), EGFRvIII (*65*), IL13Rα2 (*66*), among several others. Thus, we armored GPC2+ SyntEVs with tumor-targeting ability achieved through binding to a second tumor antigen, GD2, and demonstrated the ability of the

anti-GD2 SyntEVs to decorate neuroblastoma cells with GPC2 proportional to GD2 abundance. In vivo systemic administration of the GD2-binding SyntEVs resulted in increased GPC2 on tumor cells and enhanced CAR T cell tumor infiltration and antitumor efficacy. Our "EV vaccination study" using the COG-N-561x model further validated the feasibility of using GPC2+ armored SyntEVs to restimulate CAR T cells in vivo weeks after initial CAR T cell administration to maintain the number of circulating CAR T cells within a therapeutic window to enable durable tumor control.

Our study has several limitations. For example, although our use of human xenograft models in immunodeficient NSG mice offers the advantage of recapitulating the human expression of tumor antigens like GPC2 and GD2, it also poses some restraints to the understanding of the full therapeutic potential of antigen-displaying SyntEVs as CAR T cell enhancers and their broader effect on endogenous immune cells. For example, ALB-binding amph-ligands (*62*) or EVs (*46*) have demonstrated trafficking to lymph nodes, where they transfer antigens to professional antigen-presenting cells. This process renders the antigen accessible for cognate CAR T cell stimulation in an optimal immune-activating environment (*62*). Thus, these studies using immunocompromised mouse models may potentially underestimate the therapeutic benefits of combining antigen-presenting SyntEVs with CAR T cells. Future studies using syngeneic neuroblastoma immunocompetent models treated with murine CAR T cells and paired antigen+ EVs are needed to fully define the effects of EV antigen presentation in a competent adaptive immune setting and additionally evaluate SyntEV-induced effects on endogenous immune cell populations. Moreover, these studies would allow verification of the hypothesis that ALB-binding SyntEVs can decorate DCs, resulting in GPC2 cross-presentation in the lymph nodes and engagement of endogenous antitumor T cells, similar to "amph-ligand" vaccines (*62*). Moreover, our single-cell functional cytokine immune profiling of GPC2 CAR T cells after exposure to GPC2-displaying SyntEVs revealed that EV stimulation induces not only secretion of effector and stimulatory cytokines, like IFN-γ and IL-2, but also chemoattractive chemokines like MIP-1α and MIP-1β, which are known to induce recruitment and activation of monocytes/macrophages and natural killer cells (*67*). These data additionally suggest that SyntEV-mediated CAR T cell activation might also stimulate recruitment and bystander activation of endogenous antitumor immune cells, further amplifying their therapeutic benefits, an effect that is best studied in immunocompetent preclinical models. Last, although we designed the studies here for stimulation of GPC2 CAR T cells in neuroblastoma, this SyntEV system can be easily adapted not only to different CAR target molecules but also to different secondary EV-targeted molecules alternative to GD2, which could be modified even during therapy. This additional engineering of EVs to display specific binding properties and target antigens may add complexity to the EV manufacturing process. However, HEK2-93T cells, which we used as SyntEV producer cells, are particularly amenable to stable genetic modifications and have been previously used to meet large-scale EV production for clinical use (*68*). Similarly to the uniCAR approach (*69*), this approach potentially allows the use of a single CAR that can be flexibly redirected toward multiple tumor targets during therapy driven by the specific binding properties of the coinfused antigen-presenting EVs.

Our studies led to the following major findings, summarized in fig. S12: (i) Neuroblastoma tumors secrete GPC2+ and GD2+ TEVs that inform tumor antigen expression and tumor burden; (ii) TEVs exposing immunotherapeutic target antigens, such as GPC2 or GD2, functionally bind to paired CAR T cells inducing T cell activation and enhanced specific cytotoxicity against neuroblastoma cells, including those with lower antigen expression; and (iii) target antigen–displaying SyntEVs can be exploited therapeutically to boost CAR T cell persistence and antitumor efficacy in solid tumors by providing peripheral CAR T cell stimulation or delivering additional antigen to the tumor to circumvent resistance from target down-regulation. Together, this study offers a proof of concept of the versatility of EV engineering as a platform for developing CAR T cell engagers with desired properties to enable development of transformative combination immunotherapeutic approaches readily adaptable to different cancer types.

MATERIALS AND METHODS

Study design

The objectives of this study were to assess the functional effects of target antigen–displaying EVs on CAR T cells and to harness their stimulatory properties to develop CAR T cell adjuvants that can overcome the therapeutic limitations of treating solid tumors. GPC2 and GD2, validated immunotherapeutic targets in neuroblastoma being evaluated in CAR T cell phase 1 clinical trials (NCT05650749 and NCT05990751), were used as model target molecules. All in vitro experiments were performed independently at least three times. In vivo experiments were performed with random assignment to treatment groups based on a predefined range of tumor size, which was used as an inclusion criterion for enrollment; animals with tumors outside this range were excluded from the study. Experiments were conducted in a blinded manner, with investigators assessing tumor growth unaware of group allocation. Sample sizes for in vivo experiments were determined on the basis of prior publications and laboratory experience, with a minimum of four mice per group. Tumor size was measured by a digital caliper. The sample and tumor size criteria used for enrollment in each experiment are indicated in the figures or corresponding figure legends. Animal experiments were conducted using protocols approved by the CHOP Institutional Animal Care and Use Committee (IACUC; protocol nos. 0643 and 1464) with adherence to the National Institutes of Health Guide for the Care and Use of Laboratory Animals accredited by the Association for Assessment and Accreditation of Laboratory Animal Care (AAALAC) and ARRIVE guidelines. Human neuroblastoma PDXs (COG-N-561x, COG-N-421x, COG-N-424x, COG-N-619x, COG-N-452x, and COG-N-496x) were acquired from the Children's Hospital of Philadelphia Neuroblastoma biobank and the Children's Oncology Group (COG) Cell Culture and Xenograft Repository (www.cccells.org) and were characterized previously (*70*). Primary human T cells to generate CAR T cells were obtained from anonymous donors through the Human Immunology Core at the University of Pennsylvania. Donors provided informed consent through the University of Pennsylvania Immunology Core (RRID:SCR_02-2380). Twelve peripheral blood samples were collected with informed consent from children without cancer under the Children's Hospital of Philadelphia Institutional Review Board protocol no. 15920. Fifteen peripheral blood samples were obtained with informed consent through postmortem blood draws from patients with neuroblastoma who died of progressive disease 1 to 6 hours after death. These samples were used to illustrate the selective presence of GPC2+ or GD2+ EVs in the peripheral blood of patients with neuroblastoma.

Statistical analysis

All statistical analyses were performed using GraphPad software. For comparisons between two groups, either a Student's t test or a Mann-Whitney test was used. For comparisons among more than two groups with one independent variable, a one-way analysis of variance (ANOVA) followed by Tukey's or Dunnett's multiple comparisons test was applied, as indicated in the figure legends. Survival curves were generated using the Kaplan-Meier method and compared using the log-rank (Mantel-Cox) test. All tests were two sided, and statistical significance was defined as $P < 0.05$. No additional adjustments to alpha levels were made for multiple testing beyond the post hoc corrections specified. The exact statistical test and number of replicates (n) are reported in the respective figures or figure legends. All individual-level data for experiments with $n < 20$ are available in data file S1.

Supplementary Materials

The PDF file includes:
Materials and Methods
Figs. S1 to S12
References (*71*–*73*)

Other Supplementary Material for this manuscript includes the following:
Data file S1
MDAR Reproducibility Checklist

REFERENCES AND NOTES

1. S. L. Maude, T. W. Laetsch, J. Buechner, S. Rives, M. Boyer, H. Bittencourt, P. Bader, M. R. Verneris, H. E. Stefanski, G. D. Myers, M. Qayed, B. De Moerloose, H. Hiramatsu, K. Schlis, K. L. Davis, P. L. Martin, E. R. Nemecek, G. A. Yanik, C. Peters, A. Baruchel, N. Boissel, F. Mechinaud, A. Balduzzi, J. Krueger, C. H. June, B. L. Levine, P. Wood, T. Taran, M. Leung, K. T. Mueller, Y. Zhang, K. Sen, D. Lebwohl, M. A. Pulsipher, S. A. Grupp, Tisagenlecleucel in children and young adults with B-cell lymphoblastic leukemia. *N. Engl. J. Med.* **378**, 439–448 (2018).
2. A. J. Hou, L. C. Chen, Y. Y. Chen, Navigating CAR-T cells through the solid-tumour microenvironment. *Nat. Rev. Drug Discov.* **20**, 531–550 (2021).
3. R. G. Majzner, C. L. Mackall, Tumor antigen escape from CAR T-cell therapy. *Cancer Discov.* **8**, 1219–1226 (2018).
4. F. Marofi, R. Motavalli, V. A. Safonov, L. Thangavelu, A. V. Yumashev, M. Alexander, N. Shomali, M. S. Chartrand, Y. Pathak, M. Jarahian, S. Izadi, A. Hassanzadeh, N. Shirafkan, S. Tahmasebi, F. M. Khiavi, CAR T cells in solid tumors: Challenges and opportunities. *Stem Cell Res. Ther.* **12**, 81 (2021).
5. G. Chen, A. C. Huang, W. Zhang, G. Zhang, M. Wu, W. Xu, Z. Yu, J. Yang, B. Wang, H. Sun, H. Xia, Q. Man, W. Zhong, L. F. Antelo, B. Wu, X. Xiong, X. Liu, L. Guan, T. Li, S. Liu, R. Yang, Y. Lu, L. Dong, S. McGettigan, R. Somasundaram, R. Radhakrishnan, G. Mills, Y. Lu, J. Kim, Y. H. Chen, H. Dong, Y. Zhao, G. C. Karakousis, T. C. Mitchell, L. M. Schuchter, M. Herlyn, E. J. Wherry, X. Xu, W. Guo, Exosomal PD-L1 contributes to immunosuppression and is associated with anti-PD-1 response. *Nature* **560**, 382–386 (2018).
6. M. Poggio, T. Hu, C. C. Pai, B. Chu, C. D. Belair, A. Chang, E. Montabana, U. E. Lang, Q. Fu, L. Fong, R. Blelloch, Suppression of exosomal PD-L1 induces systemic anti-tumor immunity and memory. *Cell* **177**, 414–427.e13 (2019).
7. V. M. Ukrainskaya, O. E. Musatova, D. V. Volkov, D. S. Osipova, D. S. Pershin, A. M. Moysenovich, E. G. Evtushenko, E. A. Kulakovskaya, E. G. Maksimov, H. Zhang, Y. P. Rubtsov, M. A. Maschan, A. V. Stepanov, A. G. Gabibov, CAR-tropic extracellular vesicles carry tumor-associated antigens and modulate CAR T cell functionality. *Sci. Rep.* **13**, 463 (2023).
8. A. E. Russell, A. Sneider, K. W. Witwer, P. Bergese, S. N. Bhattacharyya, A. Cocks, E. Cocucci, U. Erdbrugger, J. M. Falcon-Perez, D. W. Freeman, T. M. Gallagher, S. Hu, Y. Huang, S. M. Jay, S. I. Kano, G. Lavieu, A. Leszczynska, A. M. Llorente, Q. Lu, V. Mahairaki, D. C. Muth, N. Noren Hooten, M. Ostrowski, I. Prada, S. Sahoo, T. H. Schoyen, L. Sheng, D. Tesch, G. Van Niel, R. E. Vandenbroucke, F. J. Verweij, A. V. Villar, M. Wauben, A. M. Wehman, H. Yin, D. R. F. Carter, P. Vader, Biological membranes in EV biogenesis, stability, uptake, and cargo transfer: An ISEV position paper arising from the ISEV membranes and EVs workshop. *J. Extracell. Vesicles* **8**, 1684862 (2019).
9. J. Wolfers, A. Lozier, G. Raposo, A. Regnault, C. Thery, C. Masurier, C. Flament, S. Pouzieux, F. Faure, T. Tursz, E. Angevin, S. Amigorena, L. Zitvogel, Tumor-derived exosomes are a source of shared tumor rejection antigens for CTL cross-priming. *Nat. Med.* **7**, 297–303 (2001).
10. J. W. Kim, E. Wieckowski, D. D. Taylor, T. E. Reichert, S. Watkins, T. L. Whiteside, Fas ligand-positive membranous vesicles isolated from sera of patients with oral cancer induce apoptosis of activated T lymphocytes. *Clin. Cancer Res.* **11**, 1010–1020 (2005).
11. F. Ma, J. Vayalil, G. Lee, Y. Wang, G. Peng, Emerging role of tumor-derived extracellular vesicles in T cell suppression and dysfunction in the tumor microenvironment. *J. Immunother. Cancer* **9**, e003217 (2021).
12. X. Liu, C. A. Wills, L. Chen, J. Zhang, Y. Zhao, M. Zhou, J. M. Sundstrom, T. Schell, V. S. Spiegelman, M. M. Young, H. G. Wang, Small extracellular vesicles induce resistance to anti-GD2 immunotherapy unveiling tipifarnib as an adjunct to neuroblastoma immunotherapy. *J. Immunother. Cancer* **10**, e004399 (2022).
13. M. Barok, M. Puhka, N. Yazdi, H. Joensuu, Extracellular vesicles as modifiers of antibody-drug conjugate efficacy. *J. Extracell. Vesicles* **10**, e12070 (2021).
14. W. Zhong, Z. Xiao, Z. Qin, J. Yang, Y. Wen, Z. Yu, Y. Li, N. C. Sheppard, S. Y. Fuchs, X. Xu, M. Herlyn, C. H. June, E. Pure, W. Guo, Tumor-derived small extracellular vesicles inhibit the efficacy of CAR T cells against solid tumors. *Cancer Res.* **83**, 2790–2806 (2023).
15. R. G. Majzner, J. S. Simon, J. F. Grosso, D. Martinez, B. R. Pawel, M. Santi, M. S. Merchant, B. Geoerger, I. Hezam, V. Marty, P. Vielh, M. Daugaard, P. H. Sorensen, C. L. Mackall, J. M. Maris, Assessment of programmed death-ligand 1 expression and tumor-associated immune cells in pediatric cancer tissues. *Cancer* **123**, 3807–3815 (2017).
16. K. K. Matthay, J. M. Maris, G. Schleiermacher, A. Nakagawara, C. L. Mackall, L. Diller, W. A. Weiss, Neuroblastoma. *Nat. Rev. Dis. Primers* **2**, 16078 (2016).
17. K. R. Bosse, P. Raman, Z. Zhu, M. Lane, D. Martinez, S. Heitzeneder, K. S. Rathi, N. M. Kendsersky, M. Randall, L. Donovan, S. Morrissy, R. T. Sussman, D. V. Zhelev, Y. Feng, Y. Wang, J. Hwang, G. Lopez, J. L. Harenza, J. S. Wei, B. Pawel, T. Bhatti, M. Santi, A. Ganguly, J. Khan, M. A. Marra, M. D. Taylor, D. S. Dimitrov, C. L. Mackall, J. M. Maris, Identification of GPC2 as an oncoprotein and candidate immunotherapeutic target in high-risk neuroblastoma. *Cancer Cell* **32**, 295–309.e12 (2017).
18. M. Sun, Y. Cao, R. Okada, J. M. Reyes-Gonzalez, H. G. Stack, H. Qin, N. Li, C. Seibert, M. C. Kelly, E. Ruppin, M. Ho, C. J. Thiele, R. Nguyen, Preclinical optimization of a GPC2-targeting CAR T-cell therapy for neuroblastoma. *J. Immunother. Cancer* **11**, e005881 (2023).
19. G. Pascual-Pasto, B. McIntyre, M. G. Hines, A. M. Giudice, L. Garcia-Gerique, J. Hoffmann, P. Mishra, S. Matlaga, S. Lombardi, R. Shraim, P. M. Schurch, M. Yarmarkovich, T. J. Hofmann, F. Alikarami, D. Martinez, M. Tsang, L. Gil-de-Gomez, T. T. Spear, K. M. Bernt, A. J. Wolpaw, D. S. Dimitrov, W. Li, K. R. Bosse, CAR T-cell-mediated delivery of bispecific innate immune cell engagers for neuroblastoma. *Nat. Commun.* **15**, 7141 (2024).
20. G. Pascual-Pasto, B. McIntyre, A. M. Giudice, F. Alikarami, A. Morrissey, S. Matlaga, T. J. Hofmann, V. Burgueno, K. Harvey, D. Martinez, A. C. Shah, J. B. Foster, J. Pogoriler, R. C. Eagle, A. M. Carcaboso, C. L. Shields, A. M. Leahey, K. R. Bosse, Targeting GPC2 on intraocular and CNS metastatic retinoblastomas with local and systemic delivery of CAR T-cells. *Clin. Cancer Res.* **30**, 3578–3591 (2024).
21. S. Heitzeneder, K. R. Bosse, Z. Zhu, D. Zhelev, R. G. Majzner, M. T. Radosevich, S. Dhingra, E. Sotillo, S. Buongervino, G. Pascual-Pasto, E. Garrigan, P. Xu, J. Huang, B. Salzer, A. Delaidelli, S. Raman, H. Cui, B. Martinez, S. J. Bornheimer, B. Sahaf, A. Alag, I. S. Fetahu, M. Hasselblatt, K. R. Parker, H. Anbunathan, J. Hwang, M. Huang, K. Sakamoto, N. J. Lacayo, D. D. Klysz, J. Theruvath, J. G. Vilches-Moure, A. T. Satpathy, H. Y. Chang, M. Lehner, S. Taschner-Mandl, J. P. Julien, P. H. Sorensen, D. S. Dimitrov, J. M. Maris, C. L. Mackall, GPC2-CAR T cells tuned for low antigen density mediate potent activity against neuroblastoma without toxicity. *Cancer Cell* **40**, 53–69.e9 (2022).
22. J. B. Foster, C. Griffin, J. L. Rokita, A. Stern, C. Brimley, K. Rathi, M. V. Lane, S. N. Buongervino, T. Smith, P. J. Madsen, D. Martinez, A. Delaidelli, P. H. Sorensen, R. J. Wechsler-Reya, K. Kariko, P. B. Storm, D. M. Barrett, A. C. Resnick, J. M. Maris, K. R. Bosse, Development of GPC2-directed chimeric antigen receptors using mRNA for pediatric brain tumors. *J. Immunother. Cancer* **10**, e004450 (2022).
23. F. Del Bufalo, B. De Angelis, I. Caruana, G. Del Baldo, M. A. De Ioris, A. Serra, A. Mastronuzzi, M. G. Cefalo, D. Pagliara, M. Amicucci, G. L. Pira, G. Leone, V. Bertaina, M. Sinibaldi, S. Di Cecca, M. Guercio, Z. Abbaszadeh, L. Iaffaldano, M. Gunetti, S. Iacovelli, R. Bugianesi, S. Macchia, M. Algeri, P. Merli, F. Galaverna, R. Abbas, M. C. Garganese, M. F. Villani, G. S. Colafati, F. Bonetti, M. Rabusin, K. Perruccio, V. Folsi, C. Quintarelli, F. Locatelli, Precision Medicine Team–IRCCS Ospedale Pediatrico Bambino Gesù, GD2-CART01 for relapsed or refractory high-risk neuroblastoma. *N. Engl. J. Med.* **388**, 1284–1295 (2023).
24. R. G. Majzner, S. Ramakrishna, K. W. Yeom, S. Patel, H. Chinnasamy, L. M. Schultz, R. M. Richards, L. Jiang, V. Barsan, R. Mancusi, A. C. Geraghty, Z. Good, A. Y. Mochizuki, S. M. Gillespie, A. M. S. Toland, J. Mahdi, A. Reschke, E. H. Nie, I. J. Chau, M. C. Rotiroti, C. W. Mount, C. Baggott, S. Mavroukakis, E. Egeler, J. Moon, C. Erickson, S. Green, M. Kunicki, M. Fujimoto, Z. Ehlinger, W. Reynolds, S. Kurra, K. E. Warren, S. Prabhu, H. Vogel, L. Rasmussen, T. T. Cornell, S. Partap, P. G. Fisher, C. J. Campen, M. G. Filbin,

G. Grant, B. Sahaf, K. L. Davis, S. A. Feldman, C. L. Mackall, M. Monje, GD2-CAR T cell therapy for H3K27M-mutated diffuse midline gliomas. *Nature* **603**, 934–941 (2022).
25. C.-H. Li, S. Sharma, A. A. Heczey, M. L. Woods, D. H. M. Steffin, C. U. Louis, B. J. Grilley, S. G. Thakkar, M. Wu, T. Wang, C. M. Rooney, M. K. Brenner, H. E. Heslop, Long-term outcomes of GD2-directed CAR-T cell therapy in patients with neuroblastoma. *Nat. Med.* **31**, 1125–1129 (2025).
26. T. Yan, L. Zhu, J. Chen, Current advances and challenges in CAR T-Cell therapy for solid tumors: Tumor-associated antigens and the tumor microenvironment. *Exp. Hematol. Oncol.* **12**, 14 (2023).
27. N. Tumino, G. Weber, F. Besi, F. Del Bufalo, V. Bertaina, P. Paci, L. Quatrini, L. Antonucci, M. Sinibaldi, C. Quintarelli, E. Maggi, B. De Angelis, F. Locatelli, L. Moretta, P. Vacca, I. Caruana, Polymorphonuclear myeloid-derived suppressor cells impair the anti-tumor efficacy of GD2.CAR T-cells in patients with neuroblastoma. *J. Hematol. Oncol.* **14**, 191 (2021).
28. P. Chhoy, C. W. Brown, J. J. Amante, A. M. Mercurio, Protocol for the separation of extracellular vesicles by ultracentrifugation from in vitro cell culture models. *STAR Protoc.* **2**, 100303 (2021).
29. K. W. Witwer, D. C. Goberdhan, L. O'Driscoll, C. Théry, J. A. Welsh, C. Blenkiron, E. I. Buzás, D. D. Vizio, U. Erdbrügger, J. M. Falcón-Pérez, Q.-L. Fu, A. F. Hill, M. Lenassi, J. Lötvall, R. Nieuwland, T. Ochiya, S. Rome, S. Sahoo, L. Zheng, Updating MISEV: Evolving the minimal requirements for studies of extracellular vesicles. *J. Extracell. Vesicles* **10**, e12182 (2021).
30. J. Chen, J. Yang, W. Wang, D. Guo, C. Zhang, S. Wang, X. Lu, X. Huang, P. Wang, G. Zhang, J. Zhang, J. Wang, Z. Cai, Tumor extracellular vesicles mediate anti-PD-L1 therapy resistance by decoying anti-PD-L1. *Cell. Mol. Immunol.* **19**, 1290–1301 (2022).
31. S. Sengupta, S. Das, A. C. Crespo, A. M. Cornel, A. G. Patel, N. R. Mahadevan, M. Campisi, A. K. Ali, B. Sharma, J. H. Rowe, H. Huang, D. N. Debruyne, E. D. Cerda, M. Krajewska, R. Dries, M. Chen, S. Zhang, L. Soriano, M. A. Cohen, R. Versteeg, R. Jaenisch, S. Spranger, R. Romee, B. C. Miller, D. A. Barbie, S. Nierkens, M. A. Dyer, J. Lieberman, R. E. George, Mesenchymal and adrenergic cell lineage states in neuroblastoma possess distinct immunogenic phenotypes. *Nat. Cancer* **3**, 1228–1246 (2022).
32. M. Gautier, C. Thirant, O. Delattre, I. Janoueix-Lerosey, Plasticity in neuroblastoma cell identity defines a noradrenergic-to-mesenchymal transition (NMT). *Cancers* **13**, 2904 (2021).
33. A. J. Wolpaw, L. D. Grossmann, J. L. Dessau, M. M. Dong, B. J. Aaron, P. A. Brafford, D. Volgina, G. Pascual-Pasto, A. Rodriguez-Garcia, Y. Uzun, M. Arsenian-Henriksson, D. J. Powell Jr., K. R. Bosse, A. Kossenkov, K. Tan, M. D. Hogarty, J. M. Maris, C. V. Dang, Epigenetic state determines inflammatory sensing in neuroblastoma. *Proc. Natl. Acad. Sci. U.S.A.* **119**, e2102358119 (2022).
34. M. Gartlgruber, A. K. Sharma, A. Quintero, D. Dreidax, S. Jansky, Y. G. Park, S. Kreth, J. Meder, D. Doncevic, P. Saary, U. H. Toprak, N. Ishaque, E. Afanasyeva, E. Wecht, J. Koster, R. Versteeg, T. G. P. Grunewald, D. T. W. Jones, S. M. Pfister, K. O. Henrich, J. van Nes, C. Herrmann, F. Westermann, Super enhancers define regulatory subtypes and cell identity in neuroblastoma. *Nat. Cancer* **2**, 114–128 (2021).
35. K. O. McNerney, S. Karageorgos, G. M. Ferry, A. J. Wolpaw, C. Burudpakdee, P. Khurana, C. N. Toland, R. Vemu, A. Vu, M. D. Hogarty, H. Bassiri, *TH-MYCN* tumors, but not tumor-derived cell lines, are adrenergic lineage, GD2+, and responsive to anti-GD2 antibody therapy. *Oncoimmunology* **11**, 2075204 (2022).
36. N. M. Kendsersky, M. Odrobina, N. W. Mabe, A. Farrel, L. Grossmann, M. Tsang, D. Groff, A. J. Wolpaw, A. Narch, F. Zammarchi, P. H. van Berkel, C. V. Dang, Y. P. Mosse, K. Stegmaier, J. M. Maris, Lineage-dependence of the neuroblastoma surfaceome defines tumor cell state-dependent and -independent immunotherapeutic targets. *Neuro Oncol.* **27**, 1372–1384 (2025).
37. F. M. Vega, A. Colmenero-Repiso, M. A. Gomez-Munoz, I. Rodriguez-Prieto, D. Aguilar-Morante, G. Ramirez, C. Marquez, R. Cabello, R. Pardal, CD44-high neural crest stem-like cells are associated with tumour aggressiveness and poor survival in neuroblastoma tumours. *EBioMedicine* **49**, 82–95 (2019).
38. S. A. Melo, L. B. Luecke, C. Kahlert, A. F. Fernandez, S. T. Gammon, J. Kaye, V. S. LeBleu, E. A. Mittendorf, J. Weitz, N. Rahbari, C. Reissfelder, C. Pilarsky, M. F. Fraga, D. Piwnica-Worms, R. Kalluri, Glypican-1 identifies cancer exosomes and detects early pancreatic cancer. *Nature* **523**, 177–182 (2015).
39. M. Mauro, P. Ugo, Z. Walton, S. Ali, C. Rastellini, L. Cicalese, Glypican-3 (GPC-3) structural analysis and cargo in serum small extracellular vesicles of hepatocellular carcinoma patients. *Int. J. Mol. Sci.* **24**, 10922 (2023).
40. C. S. Hong, B. Diergaarde, T. L. Whiteside, Small extracellular vesicles in plasma carry luminal cytokines that remain undetectable by antibody-based assays in cancer patients and healthy donors. *BJC Rep.* **2**, 16 (2024).
41. C. Tu, Z. Du, H. Zhang, Y. Feng, Y. Qi, Y. Zheng, J. Liu, J. Wang, Endocytic pathway inhibition attenuates extracellular vesicle-induced reduction of chemosensitivity to bortezomib in multiple myeloma cells. *Theranostics* **11**, 2364–2380 (2021).
42. F. Teng, M. Fussenegger, Shedding light on extracellular vesicle biogenesis and bioengineering. *Adv. Sci.* **8**, 2003505 (2020).
43. M. Catalano, L. O'Driscoll, Inhibiting extracellular vesicles formation and release: A review of EV inhibitors. *J. Extracell. Vesicles* **9**, 1703244 (2020).
44. A. Jonsson, J. Dogan, N. Herne, L. Abrahmsen, P. A. Nygren, Engineering of a femtomolar affinity binding protein to human serum albumin. *Protein Eng. Des. Sel.* **21**, 515–527 (2008).
45. J. Nilvebrant, S. Hober, The albumin-binding domain as a scaffold for protein engineering. *Comput. Struct. Biotechnol. J.* **6**, e201303009 (2013).
46. X. Liang, Z. Niu, V. Galli, N. Howe, Y. Zhao, O. P. B. Wiklander, W. Zheng, R. J. Wiklander, G. Corso, C. Davies, J. Hean, E. Kyriakopoulou, D. R. Mamand, R. Amin, J. Z. Nordin, D. Gupta, S. E. Andaloussi, Extracellular vesicles engineered to bind albumin demonstrate extended circulation time and lymph node accumulation in mouse models. *J. Extracell. Vesicles* **11**, e12248 (2022).
47. B. B. Duncan, C. E. Dunbar, K. Ishii, Applying a clinical lens to animal models of CAR-T cell therapies. *Mol. Ther. Methods Clin. Dev.* **27**, 17–31 (2022).
48. S. M. Albelda, CAR T cell therapy for patients with solid tumours: Key lessons to learn and unlearn. *Nat. Rev. Clin. Oncol.* **21**, 47–66 (2024).
49. K. R. Bosse, A. M. Giudice, M. V. Lane, B. McIntyre, P. M. Schurch, G. Pascual-Pasto, S. N. Buongervino, S. Suresh, A. Fitzsimmons, A. Hyman, M. Gemino-Borromeo, J. Saggio, E. R. Berko, A. A. Daniels, J. Stundon, M. Friedrichsen, X. Liu, M. L. Margolis, M. M. Li, M. B. Tierno, G. R. Oxnard, J. M. Maris, Y. P. Mosse, Serial profiling of circulating tumor DNA identifies dynamic evolution of clinically actionable genomic alterations in high-risk neuroblastoma. *Cancer Discov.* **12**, 2800–2819 (2022).
50. M. J. Cox, F. Lucien, R. Sakemura, J. C. Boysen, Y. Kim, P. Horvei, C. Manriquez Roman, M. J. Hansen, E. E. Tapper, E. L. Siegler, C. Forsman, S. B. Crotts, K. J. Schick, M. Hefazi, M. W. Ruff, I. Can, M. Adada, E. Bezerra, L. A. Kankeu Fonkoua, W. K. Nevala, E. Braggio, W. Ding, S. A. Parikh, N. E. Kay, S. S. Kenderian, Leukemic extracellular vesicles induce chimeric antigen receptor T cell dysfunction in chronic lymphocytic leukemia. *Mol. Ther.* **29**, 1529–1540 (2021).
51. X. X. Tang, H. Shimada, N. Ikegaki, Macrophage-mediated anti-tumor immunity against high-risk neuroblastoma. *Genes Immun.* **23**, 129–140 (2022).
52. D. Alizadeh, R. A. Wong, S. Gholamin, M. Maker, M. Aftabizadeh, X. Yang, J. R. Pecoraro, J. D. Jeppson, D. Wang, B. Aguilar, R. Starr, C. B. Larmonier, N. Larmonier, M. H. Chen, X. Wu, A. Ribas, B. Badie, S. J. Forman, C. E. Brown, IFNγ is critical for CAR T cell-mediated myeloid activation and induction of endogenous immunity. *Cancer Discov.* **11**, 2248–2265 (2021).
53. R. Kalluri, K. M. McAndrews, The role of extracellular vesicles in cancer. *Cell* **186**, 1610–1626 (2023).
54. O. P. B. Wiklander, D. R. Mamand, D. K. Mohammad, W. Zheng, R. Jawad Wiklander, T. Sych, A. M. Zickler, X. Liang, H. Sharma, A. Lavado, J. Bost, S. Roudi, G. Corso, A. J. Lennaard, M. Abedi-Valugerdi, I. Mager, E. Alici, E. Sezgin, J. Z. Nordin, D. Gupta, A. Gorgens, S. El Andaloussi, Antibody-displaying extracellular vesicles for targeted cancer therapy. *Nat. Biomed. Eng.* **8**, 1453–1468 (2024).
55. D. M. Stranford, L. M. Simons, K. E. Berman, L. Cheng, B. N. DiBiase, M. E. Hung, J. B. Lucks, J. F. Hultquist, J. N. Leonard, Genetically encoding multiple functionalities into extracellular vesicles for the targeted delivery of biologics to T cells. *Nat. Biomed. Eng.* **8**, 397–414 (2024).
56. X. Shi, Q. Cheng, T. Hou, M. Han, G. Smbatyan, J. E. Lang, A. L. Epstein, H. J. Lenz, Y. Zhang, Genetically engineered cell-derived nanoparticles for targeted breast cancer immunotherapy. *Mol. Ther.* **28**, 536–547 (2020).
57. W. Fu, C. Lei, S. Liu, Y. Cui, C. Wang, K. Qian, T. Li, Y. Shen, X. Fan, F. Lin, M. Ding, M. Pan, X. Ye, Y. Yang, S. Hu, CAR exosomes derived from effector CAR-T cells have potent antitumour effects and low toxicity. *Nat. Commun.* **10**, 4355 (2019).
58. V. Pietrobon, L. A. Todd, A. Goswami, O. Stefanson, Z. Yang, F. Marincola, Improving CAR T-cell persistence. *Int. J. Mol. Sci.* **22**, 10828 (2021).
59. T. Gargett, W. Yu, G. Dotti, E. S. Yvon, S. N. Christo, J. D. Hayball, I. D. Lewis, M. K. Brenner, M. P. Brown, GD2-specific CAR T cells undergo potent activation and deletion following antigen encounter but can be protected from activation-induced cell death by PD-1 blockade. *Mol. Ther.* **24**, 1135–1149 (2016).
60. K. Feng, Y. Guo, H. Dai, Y. Wang, X. Li, H. Jia, W. Han, Chimeric antigen receptor-modified T cells for the immunotherapy of patients with EGFR-expressing advanced relapsed/refractory non-small cell lung cancer. *Sci. China Life Sci.* **59**, 468–479 (2016).
61. A. Mackensen, J. Haanen, C. Koenecke, W. Alsdorf, E. Wagner-Drouet, P. Borchmann, D. Heudobler, B. Ferstl, S. Klobuch, C. Bokemeyer, A. Desuki, F. Luke, N. Kutsch, F. Muller, E. Smit, P. Hillemanns, P. Karagiannis, E. Wiegert, Y. He, T. Ho, Q. Kang-Fortner, A. M. Schlitter, C. Schulz-Eying, A. Finlayson, C. Flemmig, K. Kuhlcke, L. Preussner, B. Rengstl, O. Tureci, U. Sahin, CLDN6-specific CAR-T cells plus amplifying RNA vaccine in relapsed or refractory solid tumors: The phase 1 BNT211-01 trial. *Nat. Med.* **29**, 2844–2853 (2023).
62. L. Ma, T. Dichwalkar, J. Y. H. Chang, B. Cossette, D. Garafola, A. Q. Zhang, M. Fichter, C. Wang, S. Liang, M. Silva, S. Kumari, N. K. Mehta, W. Abraham, N. Thai, N. Li, K. D. Wittrup, D. J. Irvine, Enhanced CAR-T cell activity against solid tumors by vaccine boosting through the chimeric receptor. *Science* **365**, 162–168 (2019).

63. M. Yáñez-Mó, P. R.-M. Siljander, Z. Andreu, A. B. Zavec, F. E. Borràs, E. I. Buzas, K. Buzas, E. Casal, F. Cappello, J. Carvalho, E. Colás, A. Cordeiro-da Silva, S. Fais, J. M. Falcon-Perez, I. M. Ghobrial, B. Giebel, M. Gimona, M. Graner, I. Gursel, M. Gursel, N. H. H. Heegaard, A. Hendrix, P. Kierulf, K. Kokubun, M. Kosanovic, V. Kralj-Iglic, E.-M. Krämer-Albers, S. Laitinen, C. Lässer, T. Lener, E. Ligeti, A. Linē, G. Lipps, A. Llorente, J. Lötvall, M. Manček-Keber, A. Marcilla, M. Mittelbrunn, I. Nazarenko, E. N. M. Nolte-'t Hoen, T. A. Nyman, L. O'Driscoll, M. Olivan, C. Oliveira, É. Pállinger, H. A. Del Portillo, J. Reventós, M. Rigau, E. Rohde, M. Sammar, F. Sánchez-Madrid, N. Santarém, K. Schallmoser, M. S. Ostenfeld, W. Stoorvogel, R. Stukelj, S. G. Van der Grein, M. H. Vasconcelos, M. H. M. Wauben, O. De Wever, Biological properties of extracellular vesicles and their physiological functions. *J. Extracell. Vesicles* **4**, 27066 (2015).
64. S. L. Maude, N. Frey, P. A. Shaw, R. Aplenc, D. M. Barrett, N. J. Bunin, A. Chew, V. E. Gonzalez, Z. Zheng, S. F. Lacey, Y. D. Mahnke, J. J. Melenhorst, S. R. Rheingold, A. Shen, D. T. Teachey, B. L. Levine, C. H. June, D. L. Porter, S. A. Grupp, Chimeric antigen receptor T cells for sustained remissions in leukemia. *N. Engl. J. Med.* **371**, 1507–1517 (2014).
65. D. M. O'Rourke, M. P. Nasrallah, A. Desai, J. J. Melenhorst, K. Mansfield, J. J. D. Morrissette, M. Martinez-Lage, S. Brem, E. Maloney, A. Shen, R. Isaacs, S. Mohan, G. Plesa, S. F. Lacey, J. M. Navenot, Z. Zheng, B. L. Levine, H. Okada, C. H. June, J. L. Brogdon, M. V. Maus, A single dose of peripherally infused EGFRvIII-directed CAR T cells mediates antigen loss and induces adaptive resistance in patients with recurrent glioblastoma. *Sci. Transl. Med.* **9**, eaaa0984 (2017).
66. C. E. Brown, D. Alizadeh, R. Starr, L. Weng, J. R. Wagner, A. Naranjo, J. R. Ostberg, M. S. Blanchard, J. Kilpatrick, J. Simpson, A. Kurien, S. J. Priceman, X. Wang, T. L. Harshbarger, M. D'Apuzzo, J. A. Ressler, M. C. Jensen, M. E. Barish, M. Chen, J. Portnow, S. J. Forman, B. Badie, Regression of glioblastoma after chimeric antigen receptor T-cell therapy. *N. Engl. J. Med.* **375**, 2561–2569 (2016).
67. B. G. Dorner, A. Scheffold, M. S. Rolph, M. B. Huser, S. H. Kaufmann, A. Radbruch, I. E. Flesch, R. A. Kroczek, MIP-1α, MIP-1β, RANTES, and ATAC/lymphotactin function together with IFN-γ as type 1 cytokines. *Proc. Natl. Acad. Sci. U.S.A.* **99**, 6181–6186 (2002).
68. J. Johnson, M. Shojaee, J. Mitchell Crow, R. Khanabdali, From mesenchymal stromal cells to engineered extracellular vesicles: A new therapeutic paradigm. *Front. Cell Dev. Biol.* **9**, 705676 (2021).
69. M. Bachmann, The UniCAR system: A modular CAR T cell approach to improve the safety of CAR T cells. *Immunol. Lett.* **211**, 13–22 (2019).
70. J. L. Rokita, K. S. Rathi, M. F. Cardenas, K. A. Upton, J. Jayaseelan, K. L. Cross, J. Pfeil, L. E. Egolf, G. P. Way, A. Farrel, N. M. Kendsersky, K. Patel, K. S. Gaonkar, A. Modi, E. R. Berko, G. Lopez, Z. Vaksman, C. Mayoh, J. Nance, K. McCoy, M. Haber, K. Evans, H. McCalmont, K. Bendak, J. W. Bohm, G. M. Marshall, V. Tyrrell, K. Kalletla, F. K. Braun, L. Qi, Y. Du, H. Zhang, H. B. Lindsay, S. Zhao, J. Shu, P. Baxter, C. Morton, D. Kurmashev, S. Zheng, Y. Chen, J. Bowen, A. C. Bryan, K. M. Leraas, S. E. Coppens, H. Doddapaneni, Z. Momin, W. Zhang, G. I. Sacks, L. S. Hart, K. Krytska, Y. P. Mosse, G. J. Gatto, Y. Sanchez, C. S. Greene, S. J. Diskin, O. M. Vaske, D. Haussler, J. M. Gastier-Foster, E. A. Kolb, R. Gorlick, X. N. Li, C. P. Reynolds, R. T. Kurmasheva, P. J. Houghton, M. A. Smith, R. B. Lock, P. Raman, D. A. Wheeler, J. M. Maris, Genomic profiling of childhood tumor patient-derived xenograft models to enable rational clinical trial design. *Cell Rep.* **29**, 1675–1689.e9 (2019).
71. Y. Yang, C. W. Li, L. C. Chan, Y. Wei, J. M. Hsu, W. Xia, J. H. Cha, J. Hou, J. L. Hsu, L. Sun, M. C. Hung, Exosomal PD-L1 harbors active defense function to suppress T cell killing of breast cancer cells and promote tumor growth. *Cell Res.* **28**, 862–864 (2018).
72. C. W. Mount, R. G. Majzner, S. Sundaresh, E. P. Arnold, M. Kadapakkam, S. Haile, L. Labanieh, E. Hulleman, P. J. Woo, S. P. Rietberg, H. Vogel, M. Monje, C. L. Mackall, Potent antitumor efficacy of anti-GD2 CAR T cells in H3-K27M$^+$ diffuse midline gliomas. *Nat. Med.* **24**, 572–579 (2018).
73. D. M. Walter, O. S. Venancio, E. L. Buza, J. W. Tobias, C. Deshpande, A. A. Gudiel, C. Kim-Kiselak, M. Cicchini, T. J. Yates, D. M. Feldser, Systematic in vivo inactivation of chromatin-regulating enzymes identifies Setd2 as a potent tumor suppressor in lung adenocarcinoma. *Cancer Res.* **77**, 1719–1729 (2017).

Acknowledgments: We thank L. Musante and the Extracellular Vesicle Core at the University of Pennsylvania's School of Veterinary Medicine for technical support on EV characterization. We thank S. Molugu and the Electron Microscopy Resource Lab at the University of Pennsylvania for TEM analysis of EV samples. **Funding:** This work was supported by the Rally Foundation for Childhood Cancer Research (A.M.G.), an Alex's Lemonade Stand Foundation (ALSF) 'A' Award (K.R.B.), NCI R37 CA282041 (K.R.B.), NCI K08 CA230223 (K.R.B.), RP210154 from the Cancer Prevention & Research Institute of Texas (C.P.R.), Burroughs Wellcome Fund (S.E.H.), and a Children's Hospital of Philadelphia Cell and Gene Therapy Collaborative Seed Grant (K.R.B.). The ALSF also provides support for the COG Childhood Cancer Repository (www.cccells.org). **Author contributions:** Conceptualization: A.M.G. and K.R.B. Methodology: A.M.G., G.P.P., D.G., D.M., and K.R.B. Investigation: A.M.G., S.M., S.L.R., P.M.S., G.R., B.M., G.P.G., E.C.-C., V.Z., S.L., D.M., L.A.S., E.M.B., H.F., and K.R.B. Investigation—in vitro assays: A.M.G., S.M., S.L.R., P.M.S., G.R., B.M., G.P.G., V.Z., and S.L. Investigation—flow cytometry: A.M.G., S.M., S.L.R., and G.P.G. Investigation—in vivo assays: A.M.G., S.M., and G.P.P. Investigation—computational analyses: E.C.-C. Investigation—mass spectrometry studies: A.M.G., S.M., L.A.S., E.M.B., and H.F. Investigation—immunohistochemistry assays: S.M. and D.M. Visualization: A.M.G., E.C.-C., R.S., and K.R.B. Resources: A.M.G., S.E.H., J.N., C.P.R., and K.R.B. Funding acquisition: A.M.G. and K.R.B. Supervision: A.M.G. and K.R.B. Writing—original draft: A.M.G. and K.R.B. Writing—review and editing: all authors. **Competing interests:** K.R.B. and G.P.P. have applied for patents for the discovery and development of immunotherapies for cancer, including patents related to GPC2-directed immunotherapies ("Glypican 2 as a cancer marker and therapeutic target," WIPO patent number WO2017083296A1, K.R.B.; "Chimeric antigen receptors targeting glypican 2," WIPO patent number WO2020227447A1, K.R.B; "Chimeric antigen receptors containing glypican 2 binding domains," WIPO patent number WO2021016062A1, K.R.B.; "Dual targeting of pediatric malignancies through CAR T cells secreting bispecific innate immune cell engagers (BICEs)," WIPO patent number WO2023107898A1, K.R.B. and G.P.P.). K.R.B. receives royalties from Tmunity, Kite, a Gilead Company, and ConjugateBio Inc. for licensing of GPC2-related technology and funding from Tmunity and Kite, a Gilead Company, for research on GPC2-directed immunotherapies. K.R.B. is on the ConjugateBio Scientific Advisory Board and receives consulting fees. The other authors declare that they have no competing interests. **Data and materials availability:** The mass spectrometry proteomics data have been deposited to the ProteomeXchange Consortium via the PRIDE partner repository with the dataset identifier PXD067632. Newly generated GPC2+ and GPC2− SyntEV-producer cell lines, as well as plasmid constructs used for their production, are available from the corresponding author upon completion of a material transfer agreement with the Children's Hospital of Philadelphia. There are no additional restrictions on the availability of these materials. All data associated with this study are present in the paper or the Supplementary Materials.

Submitted 13 August 2024
Resubmitted 12 May 2025
Accepted 21 October 2025
Published 19 November 2025
10.1126/scitranslmed.ads4214